INTERNATIONAL ATOMIC ENERGY AGENCY
UNITED NATIONS EDUCATIONAL, SCIENTIFIC AND CULTURAL ORGANIZATION
INTERNATIONAL CENTRE FOR THEORETICAL PHYSICS
I.C.T.P., P.O. BOX 586, 34100 TRIESTE, ITALY. CABLE CENTRATOM TRIESTE

SMR.769 - 15

WORKSHOP ON
"NON-LINEAR ELECTROMAGNETIC INTERACTIONS IN SEMICONDUCTORS"

1 - 10 AUGUST 1994

"Non-linear optical properties of quantum confined semiconductors"

C. FLYTZANIS
Laboratoire d'Optique Quantique du CNRS
Ecole Polytechnique
98128 Palaiseau Cedex
France

Chapter 8

NONLINEAR OPTICS IN QUANTUM CONFINED STRUCTURES

C. Flytzanis and J. Hutter

Laboratoire d'Optique Quantique du C. N. R. S.
Ecole Polytechnique
Palaiseau, France

1. INTRODUCTION

Wave or charge confinement are being increasingly employed [1] to enhance the efficiency of several nonlinear optical processes in view of their exploitation in devices. The purpose here is to increase the interaction length or the optical nonlinearity, respectively. As will shortly become plausible, the two confinements cannot be implemented simultaneously in the same material as they address aspects incompatible with each other. The first is achieved by

confining the interacting optical beams in guides or resonators whose minimal dimension must be larger than the optical wavelength; this constitutes the topic of the nonlinear guided optics [2] in the transparency region of the nonlinear optical materials, where the nonlinearities, even for the most favorable cases, are weak but the absorption losses can be kept minimal. The second consists in enhancing the optical nonlinearity of materials with very delocalized valence electrons, like metals, semiconductors, or conjugated polymers, by artificially confining [3–5] the valence electrons in regions much shorter than their natural delocalization length in the bulk, which extends over many unit cells or even to infinity; its most conspicuous feature is the appearance of discrete optical resonances whose position, oscillator strength, and dynamics depend on the extension of the artificial confinement, and hence can be modified to meet certain requirements. This is the topic of the nonlinear optics of quantum confined microstructures.

In the present chapter, we shall restrict ourselves to the second type of confinement or quantum confinement, and discuss its impact on the optical nonlinearities. Even so, we shall mainly concentrate our attention on the degenerate odd order optical nonlinearities and, in particular, we have singled out the optical Kerr effect related [6] to the nearly frequency degenerate third-order susceptibility $\chi^{(3)}(\omega, -\omega', \omega')$, with $\omega' \approx \omega$, to illustrate different aspects of the quantum confinement. Indeed, close to the quantum confined resonances that one ultimately wishes to exploit, the quantum confined microstructures behave as truly isolated two-level systems, and the essential nonlinear mechanism then is the saturation or bleaching of the transition, which is most efficient in the degenerate or quasi-degenerate odd order nonlinear processes, where in addition the phase-matching condition is easily satisfied in different beam configurations; evidently, the important point here is to find out under what conditions the optical Kerr effect coefficient is optimally resonant. After a brief account of the fabrication techniques and the basic quantum mechanical aspects related to confined microstructures, we proceed to discuss the behavior of the optical nonlinearities in quantum confined microstructures. Technical aspects and details will be left out as they can be found in the specialized literature.

2. NONLINEAR OPTICS IN QUANTUM CONFINED MICROSTRUCTURES

The fabrication of quantum confined microstructures makes appeal [5] to the most sophisticated technologies regarding crystal growth and deposition, and the present interest in their nonlinear optical properties is only part of very intensive and multifaceted research activity related to the longstanding question of the validity range of crystal solid state concepts and behavior, and their relation to molecular and atomic ones; this is essential in understanding and predicting the properties of crystals with extended electronic states, like metals, semiconductors, or conjugated polymers, where the electronic density distribution of the constituent elements undergoes dramatic modifications in the course of forming the crystal. The implications of these aspects in miniaturized devices can be immense. With respect to nonlinear optical devices, one of the goals in the use of the quantum confinement is to optimize the optical nonlinearity per valence electron in a given frequency or time range, as dictated by the nonlinear optical device one has in mind. Its usefulness evidently relies on the possibility of artificially modifying the material characteristics, and selectively enhancing or suppressing certain polarization mechanisms with respect to the unconfined bulk material.

In the bulk, an external electric field $\mathbf{E}$, to the extent that does not exceed the cohesive field in the material $\mathbf{E}_c$, induces a nonlinear polarization [6, 7]

$$\mathbf{P} = \chi^{(1)}\mathbf{E} + \chi^{(2)}\mathbf{EE} + \chi^{(3)}\mathbf{EEE} + \cdots, \tag{1}$$

where $\chi^{(n)}$ is the nth order susceptibility [6, 7], whose magnitude is of the order of

$$\chi^{(n)} \approx 1/E_c^{n-1}, \tag{2}$$

where $E_c \approx e/a_c^2$, where a_c, a renormalized Bohr radius, measures the extension of the valence electron wave function as is fixed by the interplay between the bulk Coulomb potential and kinetic energies. By confining the valence charges within a potential well of extension $L < 2a_c$, one enhances the kinetic energy over the Coulomb one, and the electrons then are free to move within an artificial potential well whose eigenstate spacing and dynamics depend on the extension L. Concommittantly, the coefficients $\chi^{(n)}$ in the response (1) to the external field are modified since the charge cohesion is now maintained by the confinement potential, and the expansion accordingly must be made with respect to a new parameter related to the confinement strength instead of E/E_c. We shall not pursue this argument any further except to point out that, because of the presence of interfaces that must be introduced to enforce the confinement, the electric field that polarizes the charges inside the microstructure, E_i, is also modified through the dielectric confinement that takes place, and is different from the externally applied one. This too can have a dramatic influence on the nonlinear optical response superimposed on that of the quantum confinement. The quantum and dielectric confinements are two quite distinct effects, and affect the optical nonlinearity differently as will be discussed in what follows.

2.1. Fabrication of Microstructures

The progress in the fabrication techniques [3, 5, 8] has been uneven: for confinement in one dimension in semiconductors (quantum wells), they have

reached a high degree of sophistication, while they are rudimentary for three dimensions (quantum dots) and essentially nonexistant for two dimensions (quantum wires). The situation of course will change in the near future as all these microstructures are of vital importance in science and technology. The theoretical understanding and treatment of the transport and optical properties of these microstructures has also witnessed [8] noticeable progress. Here, we shall only recall the main aspects of the fabrication techniques.

The one-dimensional confined semiconductor microstructures or quantum wells are obtained by controlling the crystal growth along a crystallographic direction to within an atomic layer. The growth proceeds by layer after layer deposition on an appropriately chosen crystalline substrate. Several techniques have now been developed, such as molecular beam epitaxy (MBE), metal organic chemical vapor deposition (MOCVD), liquid phase epitaxy (LPE), hydride vapor transport (HVT), and hot wall epitaxy (HWE). These techniques, and in particular the first two are combined with powerful *in situ* analytical ones that ensure that each atomic layer is properly deposited. Finally, confinement can also arise by the presence of local strain in the lattice, and strained quantum wells [9] are presently under intensive investigation.

The preceding techniques, which have initially been developed to obtain microstructures with quantum confinement in the growth direction, can also be extended [9] to achieve confinement in two or three directions by patterning the one-dimensional confined structure with nanoscale lithographic techniques. Unfortunately, lithographic techniques and the ensuing etching profoundly modify the characteristics of the microstructures as they introduce damage that alters the dynamics as well as structure and defect content in an uncontrolled way, such as carrier depletion, enhancement of nonradiative defects, and others. For these and other reasons, these techniques are being abandoned in favor of other more direct techniques that respect free growth in two or three crystallographic directions.

Such a method for fabrication of quantum confined microstructures in two dimensions, or quantum wires, is the use of MBE or MOCVD techniques for layer by layer growth on vicinal surfaces through nucleation in well-organized steps [10–12] on an appropriately patterned substrate. Also, growth on sidewalls of cleared and etched multiquantum well structures provide excellent channels for growth of quantum wires, but here too the removal of excess semiconductor layers poses severe problems.

For fabrication of three-dimensional quantum confined microstructures or quantum dots, the most commonly [13] used technique is more or less thermally or chemically controlled precipitation in solid or liquid matrices. In the case of solid matrices, one first forms [14–17] widely supersaturated glass melts with uniformly dispersed semiconductor clusters, such as CdS_xSe_{1-x} or CdS_xTe_{1-x}, where x varies from 1 to 0, CuCl, CuBr, and more recently also GaP. In the ensuing striking process, these clusters grow to crystallites by coalescence where larger clusters grow further at the expense of the smaller ones, and reach sizes where volume properties overtake surface properties and the solid-state–like features are acquired. Several structural techniques [13] have revealed that these crystallites beyond the nucleation stage have the same structural features as the bulk ones and, in particular, the same symmetry and lattice constants. The size distribution is to some extent controlled by the temperature and duration of the striking process, and this also fixes the color of the doped glass. Solid matrices other than glass are also being used, where the size distribution can be narrower than in glass, such as polymers or zeolites [18], but other spurious effects and nonuniformity impose severe limitations here. Nanocrystals can also be obtained [19–22] in solutions or colloids by the so-called interrupted precipitation technique, and here the size distribution can be narrower than in glass but the average size cannot be varied easily; the surface properties also are not the same as in the glass matrix. By subsequent evaporation of these liquid solutions, one has free-standing nanocrystals, which can eventually be uniformly dispersed in a gel.

In principle, similar techniques [13, 23] can be used to obtain metal quantum confined structures, but the efforts have not been successful yet. The most studied systems here are small metallic particles embedded in a solid or liquid matrix, most frequently glass or water. Incidentally, much of the impetus for the study of electron quantum confinement originated from theoretical and experimental work [23–25] on the magnetic properties of such systems. Finally, we also wish to mention that conjugated polymers to some extent can be patterned to obtain quantum confined microstructures.

2.2. Quantum Confinement

The quantum confinement and to a certain extent the dielectric confinement have a relevance only for crystals with very delocalized valence electron states, as in semiconductors, metals or conjugated polymers. The states there can be written as Bloch-band states [26]

$$\psi_{n\mathbf{k}}(\mathbf{r}) = \frac{1}{\sqrt{V_d}} e^{i\mathbf{k}\cdot\mathbf{r}} u_{n\mathbf{k}}(\mathbf{r}), \tag{3}$$

where V_d is the normalization volume in dimension d (crystal volume), $u_{n\mathbf{k}}(\mathbf{r}+\mathbf{R}) = u_{n\mathbf{k}}(\mathbf{r})$ is a real space periodic function, and $\mathbf{R}$ is any lattice vector. The corresponding band energy $E_n(\mathbf{k})$ is a reciprocal space periodic function, i.e., $E_n(\mathbf{k}+\mathbf{K}) = E_n(\mathbf{k})$ where $\mathbf{k}$ is the wavevector that labels the electron state in the band n within the first Brillouin zone (B.Z.) that has dimensions of the order of the inverse of the lattice constant. Except close to the border of the B.Z., the space periodic part $u_{n\mathbf{k}}(\mathbf{r})$ is fairly insensitive to $\mathbf{k}$ as it essentially

reflects the wavefunctions centered at the atoms within a unit cell. For most purposes, it is sufficient to only consider a two-band model, a filled valence band and an empty conduction band, separated by an energy gap E_g in the center of the Brillouin zone.

The essential aspect of (3) is that it has the form of a periodically modulated free wave and $\mathbf{k}$ is a good quantum number. In particular, close to the B.Z. center where the $\mathbf{k}$-dependence of $u_{n\mathbf{k}}$ is weak and can be disregarded, the energy spectrum is

$$E_{c,v} = \pm\left(\frac{E_g}{2} + \frac{\hbar^2}{2m^*_{c,v}}k^2\right), \tag{4}$$

namely the same as for free particles with mass m_c^* and m_v^*, which from now on will be labelled m_e^* and m_h^*, for the conduction (+) and valence (−) bands, respectively, also termed electron (negatively charged) and hole (positively charged) bands. In the case of semiconductors, the valence band is usually spin-orbit split into several subbands, the so-called light and heavy hole bands. For most purposes (see Fig. 1), the main qualitative difference between metals and semiconductors is that for semiconductors $E_g \neq 0$ and the two bands are asymmetric with respect to the Fermi level E_F as they are formed from different combinations of s- and p-type atomic wavefunctions and $m_e^* < m_h^* < m$, while for metals $E_g = 0$ and the two bands are symmetric with respect to the Fermi level as they are formed from the same combination of s-type (and eventually p-type) wavefunctions and $m_e^* = m_h^* \approx m$ (initially, one actually has a single half-filled band up to the Fermi level that for most purposes can be replaced by

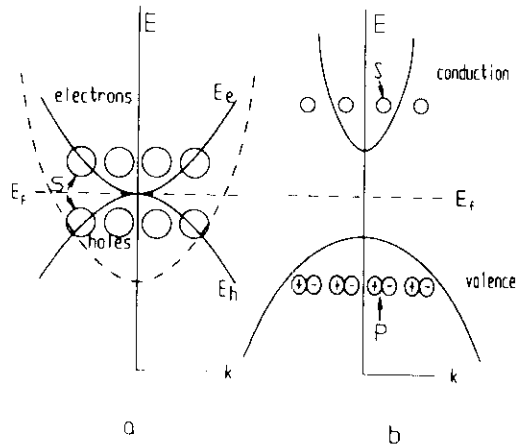

Fig. 1. Conduction (electron) and valence (hole) bands for a metal (a) and for a semiconductor (b). Also indicated are the s- and p-type orbitals that make up the band wavefuntions

an equivalent pair of parabolic bands that are mirror images to each other with respect to the Fermi level where they touch (see Fig. 1)).

Actually, the approximation (4) amounts the replacing the one-electron periodic Hamiltonian

$$H_0 = -\frac{\hbar^2}{2m}\nabla^2 + V(r) \tag{5}$$

by the free-electron and hole Hamiltonian

$$\tilde{H}_0 = -\frac{\hbar^2}{2m_e^*}\nabla_e^2 - \frac{\hbar^2}{2m_h^*}\nabla_h^2, \tag{6}$$

whose spectrum is a continuum characterized by a dimensionality d and a joint density of states that can be easily derived. Indeed, the Schrödinger equation for a particle of mass m^* in free space of dimensionality $d = 1, 2, 3$ is

$$-\frac{\hbar^2}{2m^*}\nabla_r^2\psi(r) = E\psi(\mathbf{r}),$$

and can be easily solved to obtain

$$\psi(\mathbf{r}) = \frac{1}{\sqrt{V_d}}e^{i\mathbf{k}\cdot\mathbf{r}}, \tag{7a}$$

$$E(\mathbf{k}) = \frac{\hbar^2}{2m^*}k^2, \tag{7b}$$

where $\mathbf{r}$ and $\mathbf{k}$ are vectors with d independent components, and V_d is a normalization volume in dimension d, chosen sufficiently large so that $\mathbf{k}$ can be varied continuously. The density of states at the energy E is given by

$$D_d(E) = \frac{dN_d}{dE} = \frac{dN_d}{dk}\frac{dk}{dE}, \tag{8a}$$

where

$$N_d(E) = \int_0^E d\mathbf{k} \tag{8b}$$

is the total number of states up to the level E. One gets, with allowance for spin degeneracy:

- one-dimensional (1D), $d = 1$,

$$D_1(E) = \frac{1}{\pi}\left(\frac{2m^*}{\hbar^2}\right)^{1/2}\left(E - \frac{E_0}{2}\right)^{1/2}; \tag{9a}$$

- two-dimensional (2D), $d = 2$,

$$D_2(E) = \frac{1}{2\pi}\left(\frac{2m^*}{\hbar^2}\right)\theta\left(\frac{E - E_1}{2}\right), \tag{9b}$$

where $\theta(x)$ is the Heaviside step function;

- three-dimensional (3D), $d = 3$,

$$D_3(E) = \frac{1}{2\pi^2}\left(\frac{2m^*}{\hbar^2}\right)^{3/2}\left(\frac{E - E_2}{2}\right)^{1/2}. \tag{9c}$$

where, E_0, E_1, E_2 are the gaps E_g with the appropriate dimensionality, namely a point, a line, and a surface, respectively, as specified by the topology of the critical region or Van Hove singularity [26]. In the case of metals, one sets $E_i = 0$ in (9a, b, c) but their dimensionality remains unaltered, being a topological invariant intrinsically related to the dimensionality of the electron density distribution. In Figs. 2 and 3, we schematically depict the density of states (9a, b, c).

This free electron behavior is modified by different interactions that were not included in H_0, such as:

(i) electron–electron coulomb and exchange interactions;
(ii) impurity and interface interactions;
(iii) confinement by interfaces or strain.

The first one does not affect the crystal periodicity, but the other two do. The strength of each interaction can be measured by a characteristic energy as follows.

The dominant part of the electron–electron interactions can be taken into account through the electron–hole interaction:

$$V_{eh} = -e^2/\epsilon|\mathbf{r}_e - \mathbf{r}_h|. \tag{10}$$

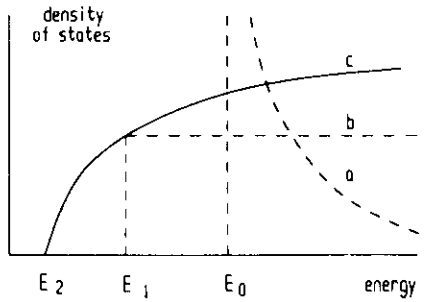

Fig. 2. Density of states for an ideal one-dimensional (a), two-dimensional (b), and three-dimensional (c) ideal semiconductor. When $E_i = 0$, the same curves are valid for an ideal metal of the same dimensionality.

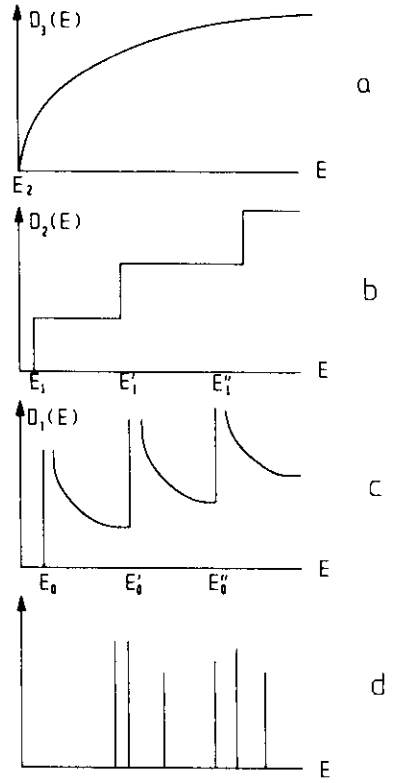

Fig. 3. Modification of the density of states of an ideal three-dimensional semiconductor (a) as it is gradually subject to one-, two-, and three-dimensional confinement (curves b, c, and d, respectively).

where ϵ is the semiconductor dielectric constant which is finite for $\mathbf{q} \to 0$ as $E_g \neq 0$. For metals, $E_g = 0$ and $\epsilon \to \infty$ as $\mathbf{q} \to 0$, and all Coulomb interactions are completely screened out within a unit cell length. As a consequence of (10), in semiconductors one may have [27] electron–hole bound pairs, or exciton states, with a binding energy of the order of

$$E_{ex} = \frac{e^2}{a_{ex}}, \tag{11}$$

where $a_{ex} = \hbar^2\epsilon/\mu e^2$ is an effective Bohr radius, with

$$1/\mu = 1/m_e^* + 1/m_h^*. \tag{12}$$

In metals, such states are absent in general because of the complete screening of the Coulomb interaction. Besides the e–h interaction (10), one may have

electron–hole pair–pair interactions that result in biexcitons with binding energy $E_{bex} < E_{ex}$, the most studied case being the biexciton in CuCl, or more complex many-body Coulomb and exchange interactions, which we do not need to specify here [28, 29].

Similarly, the electron impurity interaction in analogy to (7) may be represented with a central potential

$$V_i = \frac{e^2}{\epsilon r}, \tag{13}$$

which introduces two characteristic lengths, the hole and electron radii $a_{e,h} = \hbar^2\epsilon/m^*_{e,h}e^2$, and its strength is

$$E_{e,h} = \frac{e^2}{\epsilon a_{e,h}}, \tag{14}$$

where $a_h < a_e \approx a_{ex}$, since in general $m^*_h < m^*_e$ and the validity condition for (10) and (13) is that the unit cell dimension a is much smaller than the characteristic lengths a_h and a_e. This is the essence of the effective mass approximation [26], which amounts to representing the electron and hole wavefunctions by wave packets of Bloch states (3) with an envelope that vanishes at infinity and with the characteristic lengths just defined. These lengths are the effective Bohr radii associated with the potentials (10) and (13) and are also defined by the condition that the average value of the electron or hole kinetic energy operator (6) roughly equals to that of the potential. Thus, these characteristic lengths, or effective Bohr radii, reflect the distance at which the kinetic and potential energies balance each other or, more precisely, where the total ground state energy is minimal.

The introduction of electron confinement that restricts the envelope within a region of extension L equal to or smaller than any of these characteristic lengths $2a_c$, i.e., $L \leq 2a_c$ with $a_c = a_e$, a_h, or a_{ex}, clearly perturbs this balance since the kinetic energy, which now varies as $(a_c/L)^2$, becomes larger than the potential energy, which varies as a_c/L. The effect of the potentials (10) or (13) can then be neglected in a first approximation with respect to the kinetic energy, and the electrons and/or holes behave as free particles within the confined region. Accordingly, if we assume this to be represented by a spherical potential well of infinite height, the characteristic energy of the confinement is

$$E_c = \frac{\hbar^2}{2m^*}\frac{\pi}{L^2} = \frac{1}{2}\frac{e^2}{a_c}\left(\frac{a_c}{L}\right)^2. \tag{15}$$

The important point to notice in (15) is its dependence on a parameter, namely the length L, that can be externally modified, in contrast to the lengths a_h, a_e, and $a_{ex} \approx a_e$, which are intrinsic to the material. Thus, as L decreases E_c increases and gradually suppresses the effect of the other interactions, and eventually becomes the dominant energy term; one also says that the bound electron and hole states get ionized. The main consequence [30] is that now the initially continuous energy spectrum of the free-electron Hamiltonian (6) is radically modified and replaced by a discrete energy spectrum, namely one of quantum confined levels whose spacing depends on L, and can be accordingly modified by appropriate choice of the value of L. At the same time, the selection rules for transitions between these levels introduce fundamentally new features in the optical spectrum. In particular, the conservation of the wavevector $\mathbf{k}$, which only allows vertical optical transitions in the infinite crystal and is a consequence of the crystalline periodicity, breaks down in the confined system since the wavevector is no longer a good quantum number.

This is the essence of the quantum confinement, and its usefulness resides in the possibility of altering the energy spectrum and electron dynamics by changing the extension of the confinement. Clearly, the modifications of these features with respect to the bulk depend on the form of the confinement, its dimensionality, and its extension, but they also depend on the chemical constitution of the interface and several other aspects.

The previous approach is based on the assumption that the effective mass approximation is valid [30], and this has certain limitations, in particular regarding the inclusion of interface states, which play a major role in the relaxation but cannot be accounted for within this scheme; one can only introduce them in an *ad hoc* manner. An alternative approach would be to start from the molecular constituents and form a molecular cluster, and then study its inner and outer electronic states and supramolecular excitations as the cluster grows in size in one or more directions to recover the states of the infinitely extended crystal. In this approach, the electronic states are expanded in atomic functions and the interface states can then be properly taken into account. There exists presently a whole set of methods [31], from simple empirical to highly sophisticated *ab initio* methods, to address these problems. In principle, the two approaches, the one based on the effective mass approximation and the other on the molecular cluster, should mingle into each other but this problem has not been consistently tackled yet. Here, we shall only use the effective mass approximation to analyze and assess the impact of quantum confinement in semiconductor and metal microstructures and also conjugated polymers.

2.3. Dielectric Confinement

Along with the quantum confinement, the dielectric confinement too may substantially affect the nonlinear optical susceptibilites. The electric field that effectively polarizes the charge distribution inside a solid in general is not the

same as the externally applied field that also enters Maxwell equations. These two fields are differently weighted averages of the microscopic field inside the manner. They are identical only in the case of a uniform charge density with infinite extension, a situation that can be approached only in metals. If the charge density distribution is nonuniform, the two fields, the effective and the Maxwell or external, are different in general. Interfaces introduce nonuniformity in the charge distribution, and accordingly modify [32] the field strength distribution to the extent that this is not the same on either side of the interface. This is the origin of the dielectric confinement in microstructures; differently stated, in addition to the applied field, there is a field originating from the induced surface polarization. The derivation of the expression of the effective field in general, and inside the quantum confined microstructures in particular, is very complicated and depends on the geometry and dimensionality of the confinement. For later reference, we shall illustrate [33] this point here with the simple case of the spherical three-dimensional confinement, which will be extensively discussed later in connection with the quantum confinement (quantum dots) as well.

Let us consider metal or semiconductor particles uniformly and randomly dispersed in a transparent isotropic dielectric with dielectric constant ϵ_0, which will be assumed to be a scalar and real quantity. The particles will be assumed ideally spherical in shape with diameter $L = 2R$ that is much smaller than the optical wavelength λ. The volume concentration of these particles is $p \ll 1$, so that each crystallite is entirely surrounded by the dielectric, and the interparticle distance is large with respect to their diameter (Fig. 4).

Let α_V be the polarizability of such a crystallite of volume V, which has real and imaginary parts, i.e., $\alpha_V = \alpha_V' + i\alpha_V''$, so that we may formally define its dielectric constant ϵ by the relation

$$\epsilon_V = 1 + 4\pi\chi_V^{(1)} = 1 + 4\pi\frac{\alpha_V}{V}, \tag{16}$$

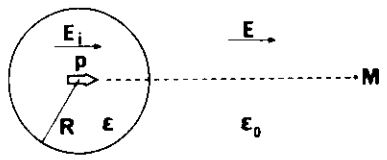

Fig. 4. A small sphere of dielectric constant ϵ and radius $R = L/2$ embedded in a matrix of dielectric constant ϵ_0 and submitted to a uniform electric field E. This leads to dielectric confinement.

which in general is expected to be a function of crystallite size and form, but here we shall identify it with the dielectric constant of its bulk, $\epsilon = \epsilon' + i\epsilon''$.

The presence of such polarizable particles modifies the dielectric constant of the composite dielectric since it results in an additional polarization

$$4\pi P \equiv (\tilde{\epsilon} - \epsilon_0)E = 3p\epsilon_0\frac{\epsilon - \epsilon_0}{\epsilon + 2\epsilon_0}E_1, \tag{17}$$

where $\tilde{\epsilon}$ is the effective dielectric constant of the composite medium and E_1 is the local field, given by $E_1 = E + \frac{4\pi P}{3\epsilon_0}$. The field inside each particle is [32]

$$E_i = \frac{3\epsilon_0}{\epsilon + 2\epsilon_0}E_1 \approx f_1 E, \tag{18}$$

and the dipole induced by the applied field $\mathbf{E}$ in a spherical particle surrounded by a dielectric is

$$P_{\text{ind}} = R^3\epsilon_0\frac{\epsilon - \epsilon_0}{\epsilon + 2\epsilon_0}E_1.$$

Inserting this in (17) and assuming $p \ll 1$, one obtains

$$\tilde{\epsilon} = \epsilon_0 + 3p\epsilon_0\frac{\epsilon - \epsilon_0}{\epsilon + 2\epsilon_0}. \tag{19}$$

This expression was initially derived by Maxwell-Garnett [34]. To the extent that ϵ is complex and frequency-dependent, we see that one has an enhancement close to a frequency ω_s such that

$$\epsilon'(\omega_s) + 2\epsilon_0 = 0. \tag{20}$$

This is the condition for the surface excitation or surface plasmon resonance; its width is determined by ϵ'', and one can also obtain the extinction coefficient

$$\alpha = p\frac{\omega}{nc}|f_1(\omega)|^2\epsilon''.$$

It is also the origin of the local field enhancement of several nonlinear optical effects in interfaces. Its impact is most striking on the nonlinear optical Kerr coefficients and below we will consider this case only [33, 35].

For this, we recall that in the presence of an intense electric field, the induced polarization may be written [6, 7]

$$\Delta\mathbf{P} = \mathbf{P}^{(1)} + \mathbf{P}^{(2)} + \mathbf{P}^{(3)} + \cdots,$$

where $\mathbf{P}^{(n)}$, $n > 1$, is the nonlinear polarization term of order n. Since the

medium is isotropic, all even order terms are zero while

$$\mathbf{P}^{(1)} = \tilde{\chi}^{(1)}\mathbf{E}, \tag{21}$$

$$\mathbf{P}^{(3)} = \tilde{\chi}^{(3)}\mathbf{EEE}, \tag{22}$$

where $\tilde{\chi}^{(1)}$ and $\tilde{\chi}^{(3)}$ are the effective linear and third-order susceptibilities of the composite, respectively, and are in general frequency-dependent. Their quantum mechanical expressions will be given in Section 2.4 For the optical Kerr effect, we are interested here in the relevant polarization induced by an intense field E of frequency ω is

$$\mathbf{P}^{(3)}(\omega) = 3\tilde{\chi}^{(3)}(\omega, -\omega, \omega)|\mathbf{E}(\omega)|^2\mathbf{E}(\omega), \tag{23}$$

and may also be described as an optically induced change of the optical dielectric constant $\delta\tilde{\epsilon} = 12\pi\tilde{\chi}^{(3)}|E(\omega)|^2$ or by differentiating (19), retaining only the contribution of the inclusions, and introducing the factor f_1 defined in (18):

$$\delta\tilde{\epsilon} = 12\pi p|f_1|^2 f_1^2\chi^{(3)}|E|^2E \tag{24}$$

or

$$\tilde{\chi}^{(3)} = p|f_1|^2 f_1^2\chi^{(3)} \tag{25}$$

where $\chi^{(3)}$ is the cubic susceptibility for an inclusion and we have dropped any reference to the frequency.

Thus, $\chi^{(3)}$ can be enhanced substantially [33, 35] if ω is close to the surface plasmon resonance, Eq. (20), in addition to the enhancement that results from quantum confined resonances of $\chi^{(3)}$. The previous derivation can be made more rigorous [36–37], and also can be extended to nonspherical particles, for instance ellipsoids, although with considerable effort and at the expense of simplicity, by introducing appropriate statistical averages or using the T-matrix approach and miscroscopic considerations for the electric fields and induced dipoles. The final conclusions and results pertinent to the experimental investigations remain the same as before. Similarly, one can extend these considerations to microstructures with two- or one-dimensional confinement. The fourth power dependence on the effective field factor f_1 in $\tilde{\chi}^{(3)}$ applies in all cases, but the actual dependence of f_1 on the dielectric constants ϵ and ϵ_0 is different for the different geometries and will not be discussed here. It is clear that the local field enhancement results from resonant behavior and can be substantial in metal inclusions, but in general much less so in semiconductors. There are also predictions [39] that one may have local field mediated intrinsic bistability. Such an effect may be difficult to observe, however, because of the large absorption that is always present whenever the local field enhancement condition (20) is satisfied.

The induced change $\delta\epsilon$ of the dielectric constant (or equivalently $\delta\tilde{\epsilon}$) as previously defined pertains to the stationary regime. Since these materials will operate in a pulsed nonstationary regime when implemented in nonlinear

devices, the temporal evolution of n_2 is of central importance and is usually described by a Debye-type equaton:

$$\frac{dn_{\mathrm{NL}}(t)}{dt} + \frac{1}{\tau}n_{\mathrm{NL}}(t) = \frac{n_2}{\tau}|E|^2; \tag{26}$$

or in integral form:

$$n_{\mathrm{NL}}(t) = \frac{n_2}{\tau}\int_{-\infty}^{t} |E(s)|^2 e^{-(t-s)/\tau}\,ds, \tag{27}$$

where τ is the decay time of the optical Kerr effect, which together with the magnitude of n_2 plays a crucial role in assessing the potential use of an optical Kerr materials.

We also wish to point out that n_2 in general is a complex quantity and therefore, in addition to its magnitude and time constant, its phase is of importance as well. Only in the extreme cases of purely dispersive and purely absorptive nonlinearity is n_2 real and imaginary, respectively. The first case occurs when ω is very far from any resonance and one then expects $\tau = 0$, while the second case occurs close to a resonance and τ then is related to the relaxation processes of the resonance. In the vicinity of a frequency ω, one defines [2] a figure of merit for each one of these extreme cases:

$$f_{\mathrm{d}} = \omega\chi^{(3)}/n_0, \tag{28}$$

$$f_{\mathrm{a}} = \chi^{(3)}/\alpha\tau, \tag{29}$$

which serve as a measure of the potential usefulness of the material in a nonlinear device operating close to the frequency ω. The important feature of these figures of merit is their independence from the valence electron density since it cancels out when the ratios (28) and (29) are taken, and hence they effectively measure the nonlinearity per valence electron; they are also renormalized to oscillator strength unity. These aspects will be better appreciated when we give the quantum mechanical expressions of the optical coefficients.

2.4. Optical Nonlinearities

In the previous section, we introduced the nonlinear susceptibilities as phenomenological coefficients of the series expansion of the induced polarization in powers of the applied electric field. Here, we wish to give their quantum mechanical expressions and, anticipating the comparative analysis that will follow, we shall do so both for an infinite (periodic) crystal and for a confined one, the latter being treated as a molecular system of size L much smaller than the wavelength of the radiation field [...] In the first case, the

electronic states are extended Bloch states, while in the second one they are localized states.

A radiation field $\mathbf{E}(\mathbf{r},t)$ couples to a material system through the interaction term in the Hamiltonian,

$$H'(\mathbf{r},t) = \mathbf{P}(\mathbf{r},t)\cdot\mathbf{E}(t), \tag{30}$$

where P is the dipolar polarization operator in the interaction representation, and it is sufficient for our purposes to only assume electron contributions there. This electron-radiation coupling induces a polarization $\Delta\mathbf{P}$ in the material, which for not too strong fields can be written as a power series expansion in the field, or

$$\Delta\mathbf{P}(\mathbf{r},t) = \mathbf{P}^{(1)}(\mathbf{r},t) + \mathbf{P}^{(2)}(\mathbf{r},t) + \mathbf{P}^{(3)}(\mathbf{r},t),$$

where

$$\mathbf{P}^{(1)}(\mathbf{r},t) = \frac{-i}{v_0}\int_{-\infty}^{t} dt_1 \langle[\mathbf{P}(\mathbf{r},t), H'(\mathbf{r},t_1)]\rangle, \tag{31}$$

$$\mathbf{P}^{(2)}(\mathbf{r},t) = \frac{(-i)^2}{v_0}\int_{-\infty}^{t} dt_1 \int_{-\infty}^{t_1} dt_2 \langle[[\mathbf{P}(\mathbf{r},t), H'(\mathbf{r},t_1)], H'(\mathbf{r},t_2)]\rangle, \tag{32}$$

$$\mathbf{P}^{(3)}(\mathbf{r},t) = \frac{(-i)^3}{v_0}\int_{-\infty}^{t} dt_1 \int_{-\infty}^{t_1} dt_2 \int_{-\infty}^{t_2} dt_3 \times \langle[[[\mathbf{P}(\mathbf{r},t), H'(\mathbf{r},t_1)], H'(\mathbf{r},t_2)]H'(\mathbf{r},t_3)]\rangle \tag{33}$$

and averages are taken over the initial density matrix operator ρ_0. If we apply Fourier analysis to the radiation field and the polarization, we obtain the standard expressions of the susceptibilities of different orders, $\chi^{(1)}(\omega)$, $\chi^{(2)}(\omega_1,\omega_2)$, and $\chi^{(3)}(\omega_1,\omega_2,\omega_3)$, from (31), (32), and (33), respectively. It is also convenient to introduce the corresponding polarizabilities $\alpha(\omega)$, $\beta(\omega_1,\omega_2)$, and $\gamma(\omega_1,\omega_2,\omega_3)$, defined by

$$\chi^{(1)}(\omega) = \frac{\alpha(\omega)}{v_0}, \tag{34}$$

$$\chi^{(2)}(\omega_1,\omega_2) = \frac{\beta(\omega_1,\omega_2)}{v_0}, \tag{35}$$

$$\chi^{(3)}(\omega_1,\omega_2,\omega_3) = \frac{\gamma(\omega_1,\omega_2,\omega_3)}{v_0}, \tag{36}$$

where v_0 is the effective volume per repeat molecular unit, which in the following will always be the unit cell of the crystal. The quantum mechanical expressions of these coefficients can be found in the literature [6, 7]. For our purposes we reproduce here only the expressions of the x-components for each electron.

For small systems of size L much smaller than the optical wavelength λ, one has

$$\alpha^{(1)}(\omega) \equiv \alpha(\omega) = \frac{1}{\hbar}\sum_{g,r} f_g\left[\frac{\mu_{gr}\mu_{rg}}{(\omega_{rg}-\omega-i\Gamma_{rg})} + \frac{\mu_{gr}\mu_{rg}}{(\omega_{rg}+\omega+i\Gamma_{rg})}\right], \tag{37}$$

$$\alpha^{(2)}(\omega_1,\omega_2) \equiv \beta(\omega_1,\omega_2) = \frac{1}{\hbar^2}\sum_{g,r,s} f_g\left[\frac{\mu_{gr}\mu_{rs}\mu_{sg}}{(\omega_{rg}-\omega_1-\omega_2-i\Gamma_{rg})(\omega_{sg}-\omega_2-i\Gamma_{sg})} + 5 \text{ terms}\right], \tag{38}$$

$$\alpha^{(3)}(\omega_1,\omega_2,\omega_3) \equiv \gamma(\omega_1,\omega_2,\omega_3) = \frac{1}{\hbar^3}\sum_{g,r,s,t} f_g \times \left[\frac{\mu_{gr}\mu_{rs}\mu_{st}\mu_{tg}}{(\omega_{rg}-i\Gamma_{rg}-\omega_1-\omega_2-\omega_3)(\omega_{sg}-i\Gamma_{sg}-\omega_2-\omega_3)(\omega_{tg}-i\Gamma_{tg}-\omega_3)} + 47 \text{ terms}\right], \tag{39}$$

where f_g is the occupation number, 0 or 1, of the lowest energy level g, $\mu = ex$ is the x component of the one-electron dipole moment operator; g, s, t, u label the states with energies E_g, E_s, E_t, E_u, respectively (g stands for the lowest energy state), $\hbar\omega_{st} = E_s - E_t$ and Γ_{st} come from the damping processes: $\Gamma_{st} = 1/T_2$ if $s \neq t$, and $\Gamma_{ss} = 1/T_1$, where T_2 and T_1 are respectively dephasing and energy relaxation times, which are different for different pairs of levels but we dropped any such reference. Sometimes it is convenient to transform these expressions by introducing

$$\pi = \frac{e}{m}\mathbf{p}, \tag{40}$$

where $\mathbf{p}$ is the momentum operator of the electron, which satisfies the identity

$$[H,\mathbf{r}] = -i\frac{\hbar}{m}\mathbf{p}. \tag{41}$$

If we take the limit $\omega_i = 0$ in expressions (37), (38), and (39), we get

$$\alpha = 2\sum_{g}{}' f_g \frac{\mu_{gr}\mu_{rg}}{E_g}, \tag{42a}$$

$$\beta = 3\sum_{g,r,s}{}' f_g\left(\frac{\mu_{gr}\mu_{rs}\mu_{sg}}{E_{rg}E_{sg}} - \mu_{gg}\sum_{s}{}'\frac{\mu_{gs}\mu_{sg}}{E_{sg}^2}\right), \tag{42b}$$

$$\gamma = 4\sum_{g,r,s,t}{}' f_g\left(\frac{\mu_{gr}\mu_{rs}\mu_{st}\mu_{tg}}{E_{rg}E_{sg}E_{tg}} - \sum_{t}{}'\frac{\mu_{gt}\mu_{tg}}{E_{tg}}\sum_{s}{}'\frac{\mu_{gs}\mu_{sg}}{E_{sg}^2}\right), \quad = 4\sum_{g} f_g\left(\sum_{r,s,t}{}'\frac{\mu_{gr}\mu_{rs}\mu_{st}\mu_{tg}}{E_{rg}E_{sg}E_{tg}} - \sum_{t}{}'\frac{\mu_{gt}\mu_{tg}}{E_{tg}}\sum_{s}{}'\frac{\mu_{gs}\mu_{sg}}{E_{sg}^2}\right), \tag{42c}$$

where $\sum'$ means that the terms with $E_{sg} = 0$, etc., will be excluded from the summation. These coefficients are also related to the electric field induced shifts in the energy of the ground state g. Throughout the previous discussion, for simplicity, we assumed that kT, where T is the temperature, is much smaller than any electronic transition energy $\hbar\omega_{sg}$, so that thermodynamic considerations will not enter the picture; we recall that we are neglecting all contributions to the response from degrees of freedom other than electronic.

For systems with infinitely extended electronic states, like the Bloch-band states in bulk crystals, some care must be given in the use of the dipolar interaction Hamiltonian (30) as a perturbation since the matrix elements of the dipole moment operator $\boldsymbol{\mu} = e\mathbf{r}$ between states within the same band, the so-called intraband elements, are singular and can only be defined in terms of distributions. Without going into details, one can indeed show [40] that

$$\int \phi^*_{n'\mathbf{k}'}(\mathbf{r})\mathbf{r}\phi_{n\mathbf{k}}(\mathbf{r})\,d\mathbf{r} = -i\nabla_{\mathbf{k}}\Delta_{n'n}(\mathbf{k}',\mathbf{k}) + \delta(\mathbf{k}-\mathbf{k}')\Omega'_{n'n}(\mathbf{k}), \tag{43}$$

where

$$\Delta_{n'n}(\mathbf{k}',\mathbf{k}) = \int \phi^*_{n'\mathbf{k}'}(\mathbf{r})\phi_{n\mathbf{k}}(\mathbf{r})\,d\mathbf{r}$$

and

$$\Omega_{n'n}(\mathbf{k}) = i\int_{\text{u.c.}} u^*_{n\mathbf{k}}\nabla_{\mathbf{k}}u_{n\mathbf{k}}\,d\tau, \tag{44}$$

where $d\tau$ stands for integration over a unit cell only so that the order of magnitude of $\Omega_{n'n}$ is the dimension of the unit cell, i.e., $\Omega_{n'n} \approx a$, which is also the extension of the atomic wave functions that constitute the basis set of the bands. Thus, $e\Omega_{n'n}$ is of the order of an atomic transition dipole moment. For the interband terms, $n \neq n'$, the first term in (43) vanishes, but for the intraband ones, $n = n'$, this term introduces a highly singular behavior. One way to circumvent this problem is to go over to the momentum operator $\mathbf{p}$ whose intraband terms are zero, but this causes difficulties in our later comparison of the nonlinearities of the bulk crystal [41] with those of a microstructure of the same material, the latter being expressed in terms of μ; evidently, one may revert [42] to the $\mathbf{r}$-operator elements but this is exceedingly cumbersome. An alternative and very elegant approach is the one devised by Genkin and Mednis [43], which by a proper transformation in state phase space allows one to directly derive the expressions in terms of the effective transition dipole moment matrix elements $\boldsymbol{\Omega}_{n'n}(\mathbf{k})$. We give here only the expressions [44] of the x-components of the linear, second, and third susceptibilities of a crystal in the limit of $\omega_i \to 0$ in the two-band approximation, a completely filled valence (v) and completely empty conduction (c) band:

$$\chi^{(1)} = \frac{4e^2}{\hbar V_d}\int_{\text{B.Z.}} \Omega_{\text{vc}}S_{\text{cv}}\,d\mathbf{k}; \tag{45}$$

$$\chi^{(3)} = \frac{8e^4}{\hbar^3 V_d}\int_{\text{B.Z.}} \left(\frac{1}{\omega_{\text{vc}}}\frac{\partial S_{\text{cv}}}{\partial k}\frac{\partial S_{\text{vc}}}{\partial k} - \Omega_{\text{vc}}S_{\text{cv}}S_{\text{vc}}S_{\text{cv}}\right)d\mathbf{k} \tag{46}$$

where $\hbar\omega_{\text{cv}} = E_{\text{c}} - E_{\text{v}}$ and $S_{\text{cv}} = \Omega_{\text{cv}}/\omega_{\text{cv}}$, V_d is the normalization volume, and all quantities under the integral are functions of $\mathbf{k}$ and the integrations extend over the first Brillouin zone. In setting up (46), we have assumed for simplicity that the system possesses inversion symmetry so that in particular $\chi^{(2)} = 0$. For non-centrosymmetric systems, the expression of $\chi^{(2)}$ is slightly more lengthy [44] and the second order susceptibility is different from zero, and is given by [44]

$$\chi^{(2)} = \frac{6e^3}{\hbar^2 V_d}\frac{i}{2\pi}\int_{\text{B.Z.}} \left[S_{\text{cv}}S_{\text{cv}}(\Omega_{\text{vv}} - \Omega_{\text{cc}}) - \frac{1}{2}\left(S_{\text{vc}}\frac{\partial S_{\text{cv}}}{\partial k} - \frac{\partial S_{\text{vc}}}{\partial k}S_{\text{cv}}\right)\right]d\mathbf{k} \tag{47}$$

The preceding expressions are valid for an ideal intrinsic semiconductor described with a two-band model, an empty conduction and a filled valence band. For a metal with a half-filled band, one has a contribution from the intraband motion, which for a parabolic band is that of free electrons and leads to the linear Drude dielectric constant

$$\epsilon(\omega) = 1 - \frac{\omega_{\text{p}}^2}{\omega(\omega + i/\tau_0)} \equiv \epsilon'(\omega) + i\epsilon''(\omega), \tag{48}$$

where $\omega_{\text{p}} = (4\pi e^2 N/m)^{1/2}$ is the plasma frequency, N is the total electron density within the band, and τ_0 is the electron scattering time in the bulk. We recall here only that although one obtains [45] the same expression (48) classically and quantum mechanically, the number of electrons actually involved are not the same in the two cases. There are no contributions to $\chi^{(2)}$ and $\chi^{(3)}$ from the electron motion in a single parabolic band; such contributions only arise [46] from nonparabolic bands, but even there the contribution to $\chi^{(2)}$ vanishes [43] because of time reversal symmetry. Before concluding this section and in order to prepare the ground for the following two sections, we wish to make two important general remarks concerning the expressions (45), (46), and (47).

The first remark concerns the integrations over the Brillouin zone. The main contribution to these integrals comes from a few nonoverlapping critical regions in the joint density of states, the so-called Van Hove singularities defined by

$$\nabla_{\mathbf{k}}\omega_{\text{cv}}(\mathbf{k}) = 0, \tag{49}$$

and are a point, a line, or a surface depending on the dimensionality of the electronic density distribution, since close to these regions one may assume a parabolic approximation (4) and the joint density of states there will have the behavior described by (9a), (9b), and (9c), respectively. This directly establishes [47] a relation between the odd order optical susceptibilities $\chi^{(2n+1)}$ and the topology and dimensionality of the joint density of states. To the extent that quantum confinement modifies these aspects, we expect the former to have an impact on the odd order susceptibilities. For the even order susceptibilities $\chi^{(2n)}$, as will become evident, the critical regions (49) do not play [44, 47] such a prominent role.

The second remark concerns the contribution of two competing mechanisms in $\chi^{(3)}$, which determine its magnitude and sign (compare with (46)). The first, which will be termed intraband, is connected with the first term in the integrand in (46), and arises from electric field mixing of Bloch states with wavevector conservation between the two bands and within each band (the latter being reflected by the derivatives in **k**-space). The other, which will be termed interband, is connected with the second term in the integrand in (46), and arises from electric field mixing of states across the gap with wavevector conservation. In contrast, the linear susceptibility $\chi^{(1)}$ (compare with (45)) involves only interband terms. This competition in $\chi^{(3)}$ between the inter- and intraband contributions has crucial qualitative and quantitative implications [47]. These terms can also be interpreted as displacements of opposite signs of the effective band gaps at the critical points when an electric field is applied. The interband term can be identified as the analogue of the Stark shift for atomic levels, and consists in a repulsion between valence and conduction states at each **k** and in particular at the critical regions (49). This leads to an increase of the effective energy gap there or a negative contribution to $\chi^{(3)}$, as can also be inferred from the negative sign in front of this term in the integrand in (46). The intraband term on the other hand, which is also responsible for the Franz–Keldysh effect, consists of a repulsion of the states within a single band, which results in a net repulsion of the states in the critical regions from all other states within the same band or a net attraction of the states across the gap at the critical region; this amounts to a decrease of the effective energy gap there or a positive contribution to $\chi^{(3)}$. It is quite evident that the intraband term will be dominant whenever the bands vary strongly with k (wide bands), which will be the case of very delocalized electrons. On the other hand, this contribution will be negligible for highly localized systems, and the interband term will become dominant. Clearly, these two terms have their analogue in the two terms in (46). To the extent that quantum confinement precisely affects the delocalization, we expect that the first term will be affected but not the second one or, expressed otherwise, we expect that quantum confinement has a drastically different impact on the intraband and interband terms. In particular, it is quite clear from (43) and (46) that the quantum confinement will affect inter- and intraband transition dipole moments differently, and this makes the distinction between interband and intraband confinement meaningful and will be the basis for our discussion of the optical nonlinearities in confined structures; it will be examplified by the ideal metal and semiconductor confined structures, respectively.

3. QUANTUM CONFINEMENT

We wish now to approach the quantum confinement more quantitatively than it was done in Section 2.2, and to introduce a rationale in assessing its impact on the physical properties in general and optical ones in particular. We shall concentrate our attention on aspects that are insensitive to the form of the quantum confinement, and assume [26, 30] throughout the discussion that the effective mass approximation is valid. It is sufficient to consider a single pair of bands, a conduction and a valence band; the effect of spin-orbit splitting of the valence band into several subbands can be taken into account by pairing each subband with the conduction band, and adding the spectra assuming that the pairs are not coupled. Without any other preamble and with the notations of Section 2.2, we may then represent the electron and hole states around the center of the Brillouin zone, $\mathbf{k} \approx 0$, as wave packets of Bloch-band states in the form

$$\Psi(\mathbf{r}_e, \mathbf{r}_h) = F(\mathbf{r}_e, \mathbf{r}_h) u_e(\mathbf{r}_e) u_h(\mathbf{r}_h), \tag{50}$$

where u_e and u_h are the cell periodic part of the Bloch-band states (3) for the conduction (electron) and valence (hole) bands, respectively, at $\mathbf{k} \approx 0$, and $F(\mathbf{r}_e, \mathbf{r}_h)$ is the envelope function [30, 29], which satisfies the Schrödinger equation:

$$\left(\frac{\hbar^2}{2m_e^*} \nabla_e^2 - \frac{\hbar^2}{2m_h^*} \nabla_h^2 + V_{eh} + V_{mb} + V_i + W \right) F(\mathbf{r}_e, \mathbf{r}_h) = EF(\mathbf{r}_e, \mathbf{r}_h), \tag{51}$$

where V_{eh} is the electron–hole Coulomb interaction, V_{mb} includes the residual electron and hole coulomb and exchange interactions, which here will be lumped under the term many-body effects, V_i is the electron (hole)-impurity interaction potential, and W is the confinement potential.

The solution of Eq. (51) in general can only be tackled with numerical methods and even so with limited usefulness because of the uncertainities in the definition and determination of the different potential terms in (51). However, the essential features of the quantum confinement can be even quantitatively accounted for if some simple analytical forms for these potentials are introduced, and in addition their relative strengths are properly taken into account as discussed in Section 2.2. Keeping in mind the physical systems

where the quantum confinement has any relevance, namely metals and semiconductors, and anticipating its main impact on the electron motion there, we propose to distinguish two types of quantum confinement:

- the intraband or metal (free electron) case;
- the interband or semiconductor (bound electron) case.

The first one pertains to the modification of the intraband electron motion, while the second one to that of the interband motion. This distinction is actually dictated by the nature of the electron motion that gives rise to the linear optical properties of the ideal metal and semiconductor, and in particular to their linear dielectric constant $\epsilon(\omega)$. In the nonlinear optical coefficients, however, the two types mix up and interfere in general, but the distinction there too is physically meaningful and useful.

Since we will mainly be interested in resonant behavior, the primary characteristic is evidently the probability for transition between electron–hole pair states $|\mathrm{i}\rangle$ and $|\mathrm{f}\rangle$ of energies E_i and E_f, respectively, i.e.,

$$w(\omega) = \frac{2\pi}{\hbar} |\langle \mathrm{f}|\boldsymbol{\mu}\cdot\mathbf{E}_\omega|\mathrm{i}\rangle|^2\, \delta(E_\mathrm{f} - E_\mathrm{i} - \hbar\omega), \tag{52}$$

from which one can also obtain the absorption coefficient

$$\alpha(\omega) = \frac{2\pi\hbar\omega}{nc|E_\omega|^2}\, w(\omega) = \frac{2\pi^2\hbar e^2}{ncm} N_u f\, \delta(\hbar\omega_\mathrm{fi} - \hbar\omega),$$

where N_u is the number of unit cells per unit volume, f is the oscillator strength per unit cell,

$$f = \frac{2|\langle \mathrm{f}|\boldsymbol{\epsilon}\cdot\boldsymbol{\mu}|\mathrm{i}\rangle|^2}{m\hbar\omega N_d}, \tag{53}$$

N_d is the total number of unit cells within the normalization volume V_d, and $\boldsymbol{\epsilon}$ is the polarization direction of the electric field. The oscillator strengths satisfy a sum rule, but its use gives rise to some complications because of the introduction of the effective mass. From the preceding expressions, one can directly obtain the imaginary part $\epsilon''(\omega)$ of the dielectric constant:

$$\epsilon''(\omega) = 4\pi\chi''(\omega) = A\sum_{\mathrm{f,i}} g_\mathrm{f}|\langle \mathrm{f}|\boldsymbol{\epsilon}\cdot\boldsymbol{\mu}|\mathrm{i}\rangle|^2 \rho_\mathrm{f}(1-\rho_\mathrm{i})\, \delta(E_\mathrm{fi} - \hbar\omega), \tag{54}$$

where A is a constant, g_f is the degeneracy of state, and ρ_f and ρ_i are the occupation probabilities of states f and i, respectively.

3.1. Intraband Quantum Confinement: Metal Case

In an ideal bulk metal, one has a single band half-filled up to the Fermi level E_F, and the cell periodic part $u(\mathbf{r})$ of the Bloch function (3) is usually formed

form s and eventually p orbitals. This half-filled band, for most purposes, can be replaced by an equivalent pair of parabolic bands, mirror images of each other, see Fig. 1, with the same cell periodic part $u(\mathbf{r})$, the upper one for the electrons and the lower one for holes, that touch at $\mathbf{k} = 0$ and are situated on either side of the Fermi level E_F with $m_\mathrm{e}^* = m_\mathrm{h}^* \approx m$ and $E_\mathrm{g} = 0$ in (4). The wavevector-dependent dielectric constant $\epsilon(\mathbf{k}, \omega)$ then being infinite for $\mathbf{k} = 0$, the potentials V_eh, V_mb, and V_i are completely screened out within a distance $r_\mathrm{F} = 1/k_\mathrm{F}$, the inverse of the Fermi wavevector, which is typically of the order of a few Ångströms and roughly equal to the lattice constant. Thus, the electrons and holes behave and move as free noninteracting particles over any distance in the perfect crystal if we momentarily disregard the effect of phonons and other coherence limiting processes (actually, the effect of the impurities should also be discussed separately).

The essential characteristics of such a behavior are the dimensionality and density of states, which can be easily derived from Section 2.2 if we assume complete screening of all potentials and use the free-electron Schrödinger equation (5) to describe the electron motion, i.e.,

$$D_1(E) \sim 1/\sqrt{E}, \tag{55a}$$

$$D_2(E) \sim \theta(E), \tag{55b}$$

$$D_3(E) \sim \sqrt{E}, \tag{55c}$$

for the ideal 1D, 2D, and 3D metals respectively. The quantum confinement precisely affects these two features and by the same token the intraband transition moment (43), which determines the dielectric constant and other optical coefficients.

Indeed, in the quantum confined metal, the periodicity is broken through the introduction of the potential W, which restricts the electron and hole motion within a confined region. If we assume for simplicity that the complete screening persists even in the quantum confined metal, then we may neglect all potential terms in (51) with respect to the kinetic part and the confinement potential W, so that the electron and hole motions are decoupled and within the effective mass approximation each obeys the equation

$$\left(-\frac{\hbar^2}{2m}\nabla_\mathbf{r}^2 + W\right) F_\nu(\mathbf{r}) = E_\nu F_\nu(\mathbf{r}), \tag{56}$$

where $F_\nu(\mathbf{r})$ is the one-particle envelope function and we approximate $m_\mathrm{e}^* = m_\mathrm{h}^* \approx m$; ν stands for all quantum numbers that label the state. The wavefunction for the electron and hole in such a potential well is

$$\psi_\nu(\mathbf{r}) = F_\nu(\mathbf{r})u(\mathbf{r}), \tag{57}$$

where $u(\mathbf{r})$ is the same for electrons and holes, and actually it is immaterial

whether we work in two bands or in the original half-filled band, as can be easily seen.

Although the numerical details of the spectral modifications in (56) due to the quantum confinement depend on the actual form of W, the gross features of the optical properties and the behavior of the optical coefficients $\chi^{(n)}$ can be understood without reference to a precise potential form. To fix the ideas and substantiate certain general results, however, we may refer to the simple potential forms to be discussed in Section 3.3, where the interfaces are represented with infinite height potential walls where the envelope function $F_v(r)$ must vanish. As can be inferred from the expressions of $\chi^{(n)}$, the important parameters are the:

- transition dipole moments (intraband) and selection rules;
- level spacing;
- the level broadening and lifetime.

3.1.1. *Transition Dipole Moment (Intraband)*

This concerns the dipole transition moment in a direction defined by the unit vector ϵ between a hole state and an electron state, or equivalently between an electron state below the Fermi level and an electron state above it, namely

$$\mu_{vv'}(\epsilon) \approx e\langle\psi_{ev}|\epsilon\cdot\mathbf{r}|\psi_{ev'}\rangle = e\int F_v^*(\mathbf{r})u^*(\mathbf{r})\epsilon\cdot\mathbf{r}F_{v'}(\mathbf{r})u(\mathbf{r})\,d\mathbf{r}, \tag{58}$$

where we have dropped any reference to electron and holes since the cell periodic part $u(\mathbf{r})$ is the same for both particles (see Fig. 5a). Let us set

$$\mathbf{r} = \mathbf{R} + \boldsymbol{\rho},$$

where $\mathbf{R}$ is a lattice vector situated at the center of the unit cell and $\boldsymbol{\rho}$ only varies within the unit cell, which for simplicity will be assumed centrosymmetric, which is always the case in metals, so that

$$e\int u(\boldsymbol{\rho})\epsilon\cdot\boldsymbol{\rho}u(\boldsymbol{\rho})\,d\tau = 0. \tag{59}$$

Taking into account that $F_v(\mathbf{r})$ is a slowly varying function over several unit cells while $u(\boldsymbol{\rho})$ is fast varying and concentrated within one unit cell, (58) can be approximated by

$$\mu_{vv'}(\epsilon) \approx e\int F_v^*(\mathbf{r})\epsilon\cdot\mathbf{r}F_{v'}(\mathbf{r})\,d\mathbf{r} \tag{60}$$

where a summation over lattice cell centers within the confined region was replaced by an integration over the same region. It is clear from (60) that,

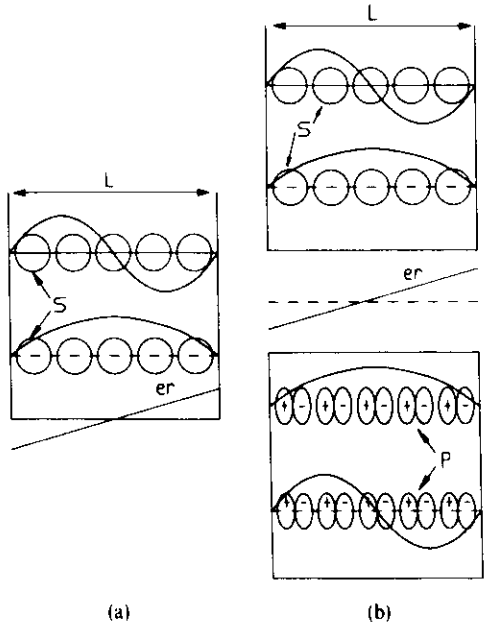

Fig. 5. Schematic view of the wavefunctions and envelopes in a quantum well used to calculate the intraband (a) and interband (b) matrix elements. Also indicated are the s- and p-type orbitals that form the basis of the wave functions.

irrespective of the actual form of W, one has

$$\mu_{vv'}(\epsilon) \approx L_\epsilon, \tag{61}$$

where L_ϵ is the extension of the confinement in the direction specified by the unit vector ϵ. This is an essential feature of the intraband confinement and is a consequence of the identification of the electron and hole cell periodic part of the wavefunction. We recall that in the infinite crystal the intraband transition dipole moment is given by (43) for $n = n'$, namely a very singular function.

3.1.2. *Level Spacing*

From the outset, the level spacing and degeneracy depend on the form of the potential W. However, apart from numerical form factors, the level spacing for large quantum numbers v varies as

$$\Delta E \sim 1/L^2, \tag{62}$$

and the density of states and degeneracy evolves to that of the free-electron system.

3.1.3. *Level Broadening and Lifetime*

Level broadening and lifetime are features entirely related to the coupling of the electron motion with the very perturbations that induce transitions between the levels, and to the extent that they depend on the phase space available and the bath to which the electron coordinates are coupled we expect that quantum confinement also affects level broadening and lifetime and modifies their bulk values. This in particular can be inferred through the drastic modification of the intraband transition dipole moments as discussed previously.

In the ideal bulk metal, the free electrons in the half-filled conduction band suffer collisions with phonons and other electrons that induce intraband transitions with a rate $1/\tau_b$, where τ_b is the mean time lapse between successive events, and will be termed scattering time; it is the time that is included in the Drude model [26,45]. In a quantum confined region of dimension $L < l_m$, where l_m is the electron mean free path, electrons in addition undergo collisions with the spherical wall at an average rate v_F/L; here v_F is the speed of the electrons close to the Fermi level E_F where the essential contribution in the quantum mechanical (one-band) Drude model for $\epsilon(\omega)$ in (48) comes from. To the extent that the two processes are uncorrelated, one may introduce an effective collision time [48]:

$$\frac{1}{\tau_{eff}} = \frac{1}{\tau_b} + \frac{v_F}{L}. \tag{63}$$

This problem has been extensively discussed [48] in the case of spherical metallic particles of diameter $L < l_m$. One also introduces a dephasing time $T_2, T_2/2 = \tau_b$, the same for all dipole allowed transitions, which leads to a homogeneous broadening of the transitions independent of the crystallite radius. Accordingly, the delta functions in (54) are replaced by Lorentzians. This classical argument is also corroborated by a detailed quantum mechanical calculation [48, 38] where, however, (63a) is only the limiting expression for $\omega \to 0$ of

$$\frac{1}{\tau_{eff}} = \frac{1}{\tau_b} + \frac{v_F}{L} g_s(v) \equiv \frac{1}{\tau_b} + \frac{v_F}{L_{eff}}, \tag{64}$$

where

$$g_s(v) = \frac{1}{v} \int_1^{\infty} x^{3/2} (x + v)^{1/2} dv \tag{65}$$

with $v = \hbar\omega / E_F$.

For a statistical assembly of metal crystallites in a dielectric, as is the case in all studied samples, one must perform an average of (54) over the size distributions $P(u)$, with $u = L/L_a$, where L_a is the average size, and $P(u)du$ is the probability of the normalized size u being in the interval du. This introduces in principle an inhomogeneous broadening, which, however, in the optical frequency range around the surface plasmon resonance ω_s defined by (20), where the level spectrum and density become essentially identical to those of the bulk metal, has effectively an inconspicuous impact on the overall broadening and can be disregarded there. This is no longer true in the far infrared, where the quantum confinement has a stronger impact but the density of states is also substantially reduced.

In addition to the dephasing mechanism of broadening, there is also an energy relaxation mechanism, which will be accounted for with a time T_1, the same for all transitions. With the introduction of these two relaxation times T_2 and T_1, which determine the dephasing and energy decay rates, respectively, one can proceed to calculate the linear and nonlinear polarizabilities using the corresponding quantum mechanical expressions.

The size-dependent broadening of the surface plasmon resonance as predicted by (63) has been experimentally confirmed [48, 38] for gold particles both in colloids and solid matrices (glass). In particular, using the experimental values for the dielectric constant for the bulk and expression (63) for the dephasing time, the variation of the absorption coefficient as a function of the average crystallite radius could be accounted for (Fig. 6). On the other hand, there is essentially little [49] or no information concerning the energy relaxation time T_1.

3.2. Interband Confinement: Semiconductor Case

In ideal bulk semiconductors, the situation at the outset is drastically different from that of metals. Here too, for most purposes, it is sufficient to use the two-band model, a filled valence and an empty conduction band on either side of the Fermi level, also designated the hole and electron bands, respectively. In contrast to the metal case, however, at $\mathbf{k} = 0$, the two bands are separated by a finite energy gap $E_g \neq 0$. Furthermore, the two bands are not symmetric with respect to the Fermi level as each originates from a different basis of atomic states, predominantly s states for the conduction band and predominantly p states for the valence band (Figs. 1 and 7). Consequently, u_c and u_h are drastically different, and in particular possess different symmetry properties. We recall that at zero temperature, the Fermi level for an intrinsic semiconductor is situated halfway between the top of the valence and the bottom of the conduction band. For states quite close to the bottom of the conduction band or to the top of the velance band, one may assume parabolic bands of the form (4) separated by a gap E_g. The essential characteristics are again the dimensionality of the electron density distribution and the joint density of states between the valence and the conduction bands. These can be

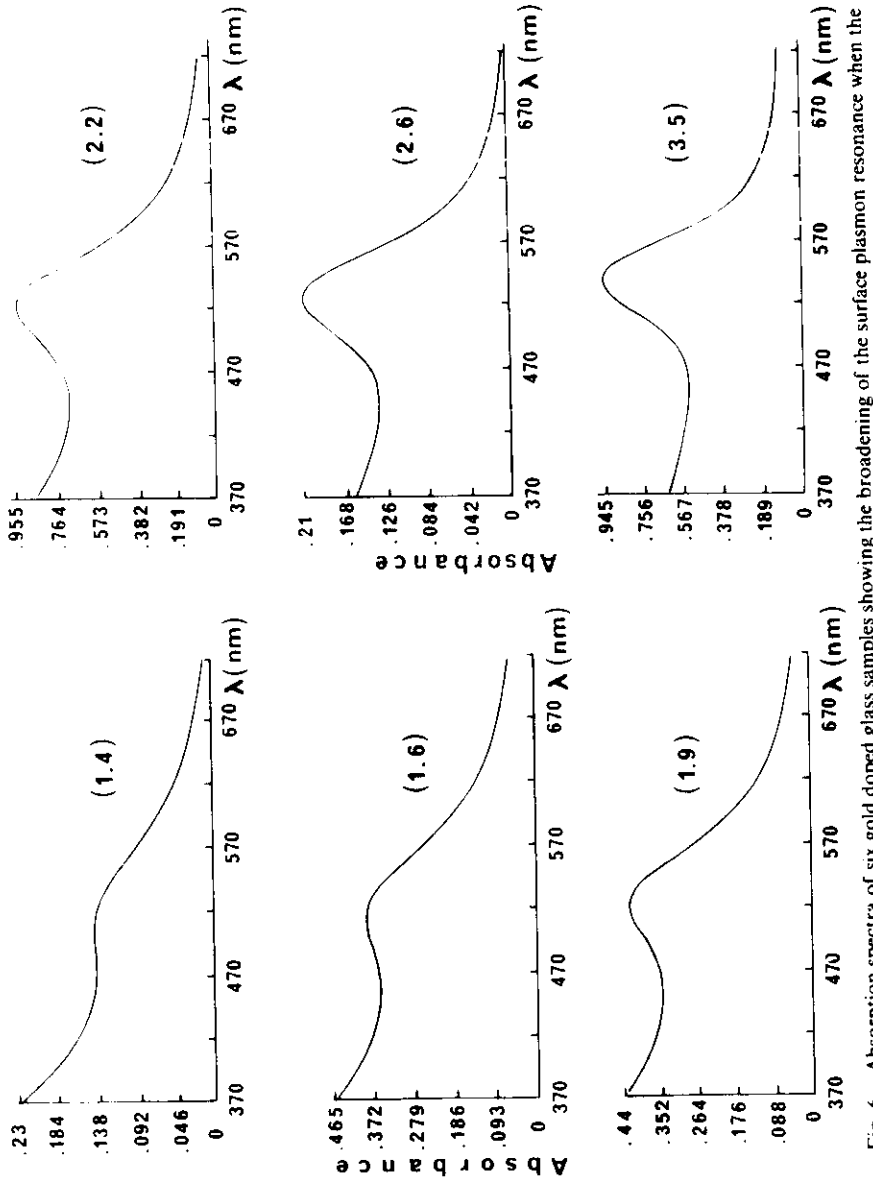

Fig. 6. Absorption spectra of six gold doped glass samples showing the broadening of the surface plasmon resonance when the radius (indicated in nm in parentheses) is reduced (from Ref. 38; see also Ref. 13).

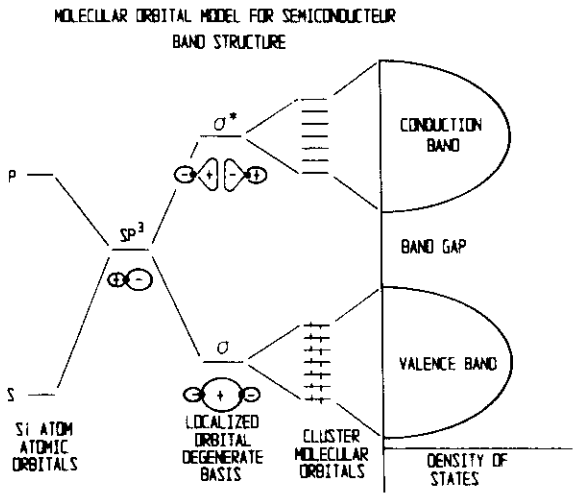

Fig. 7. Schematic view of the formation of bonds and two bands, conduction and valence, starting from a pair of *s*- and *p*-type atomic orbitals in silicium (from Ref. 70). (Reproduced with permission. © 1990 by Annual Reviews, Inc.)

easily derived from the corresponding Schrödinger equation, and by taking into account the dimensionality one has, from (9a,b,c),

$$D_1(E) \sim 1/(E - E_0)^{1/2}, \tag{66a}$$

$$D_2(E) \sim \theta(E - E_1), \tag{66b}$$

$$D_3(E) \sim (E - E_2)^{1/2}, \tag{66c}$$

for the ideal 1D, 2D, and 3D semiconductors respectively, and where E_0, E_1, and E_2 are the corresponding gaps in the Brillouin zone, a point, a line, and a surface, respectively. In actual semiconductors, the electron density distribution is not uniform. Indeed, the atomic orbitals that form the basis of the valence and conduction bands being directive and more or less strongly overlapping among themselves along certain preferential directions, the electronic density distribution possesses a quite complex topology with a superposition of 3-, 2-, and 1-dimensional features. As a matter of fact, the joint density of states of a given semiconductor is dominated by three nonoverlapping critical regions, E_0, E_1, and E_2 in k-space (Van Hove singularities), defined by the condition

$$\nabla_{\mathbf{k}}[E_c(\mathbf{k}) - E_h(\mathbf{k})] = 0,$$

and corresponding to the three cases (66a), (66b), and (66c), respectively, with $E_0 > E_1 > E_2$. In Fig. 8, we depict a fitting of the absorption spectrum of a

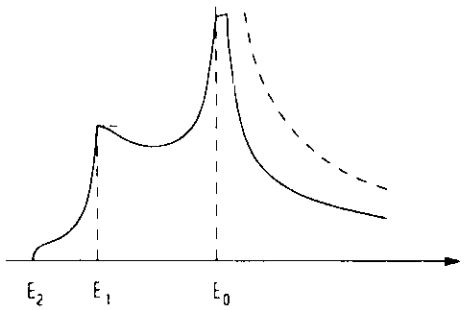

Fig. 8. Schematic view of the density of states (actually, absorption spectrum) of a real semiconductor, and its simulation as a superposition of the three ideal densities of states indicated in Fig. 2.

bulk semiconductor, which roughly also represents the joint density of states, as a superposition of the density of states of these three critical regions (66a,b,c). Since these critical regions are well separated in energy and in **k**-space, we may consider each case separately, and we shall mainly concentrate our attention on the ideal three-dimensional bulk semiconductor with free-electron and hole joint density of states given by (66c).

Because of the finite gap E_g that now separates the hole from the free-electron spectrum, the wavevector dielectric constant $\epsilon(\mathbf{k})$ is finite for $\mathbf{k} = 0$ or $\epsilon(0) = \epsilon_0$, and accordingly the screening of the electron and hole potentials V_{eh}, V_{mh}, and V_i in Eq. (51) is only partial, and bound states may exist [27] with finite extension determined by the relative strengths of the potentials. These are excitons, biexcitons, or electron and hole impurity bound states described with envelope functions of characteristic extension a_{ex}, a_e, a_h, the exciton, electron, and hole radii, respectively, with $a_{ex} \geq a_e > a_h$.

In a quantum confined semiconductor structure of extension L, the free and bound state spectrum of the bulk semiconductor is modified by the confinement in a way that depends on the strength of the quantum confinement potential relative to those of the other potentials in (51), or equivalently the confinement length L relative to the exciton, electron, and hole Bohr radii, respectively. One may then distinguish three confinement regimes [30, 50]:

Strong confinement $L/2 < a_h < a_e$. Here, all potentials in (51) in a first approximation can be neglected with respect to the kinetic part and W, the confinement potential. Hence, the electron and hole motions are decoupled, and they reduce to that of free particles of effective masses m_e^* and m_h^*, respectively, in a potential well W. The corresponding Schrödinger equation is used remembering that m must be replaced by m_e^* and m_h^*, respectively.

Intermediate confinement $a_h < a_e$. Here, the electrons can still be treated as before and their states are the same as in the strong confinement regime. For holes, on the other hand, the situation is radically different since the electron-hole interaction cannot be neglected with respect to the hole kinetic energy. Since the electrons are higher than the holes, one can assume that the adiabatic approximation applies, and proceed [50] as in the Born-Oppenheimer treatment of the nuclear motion in molecular systems.

Weak confinement $a_h < a_e < L$. For such confinement ranges, the bulk properties of the semiconductor are to a large extent established. In particular, the electron-hole potential can now allow bound electron-hole states or exciton states that are only slightly distorted with respect to those prevailing in the bulk. The essential difference with respect to the bulk is that there the exciton translational motion is confined, and this can be taken into account by treating the exciton as a free particle of mass $M = m_h^* + m_e^*$ in a potential well W of extension L. One may similarly discuss the biexciton case, but we refrain from going into such details here.

The analytical treatment of the different regimes is quite involved [50] even in the simplest case, where one assumes spherical confinement, which most closely preserves the isotropy of the bulk semiconductor. However, as in the metallic case, some gross features of the quantum confinement and its impact on the optical properties can be obtained without reference to a specific potential. In order to single out the main differences between the interband and intraband confinements, let us concentrate on the strong interband confinement regime and analyze the following features:

- transition dipole moments (interband and intraband) and selection rules;
- level spacing;
- level broadening and lifetime.

3.2.1. Transition Dipole Moments

Here, we must distinguish between intraband and interband transitions dipole moments,

$$\mu_{vv'}(\epsilon) = e \int F_v^*(\mathbf{r}) u_i^*(\mathbf{r}) \epsilon \cdot \mathbf{r} F_{v'}(\mathbf{r}) u_i(\mathbf{r})\, d\mathbf{r}, \; i = \text{e,h}, \tag{67}$$

and

$$\mu_{cv'}(\epsilon) \approx e \int F_{cv}^*(\mathbf{r}) u_e^*(\mathbf{r}) \epsilon \cdot \mathbf{r} F_{hv'}(\mathbf{r}) u_h(\mathbf{r})\, d\mathbf{r}, \tag{68}$$

respectively. The first one concerns transitions between two quantum confined electron (hole) states. Since they involve states within a single band (the

conduction or valence band), the cell periodic part u_i is the same, and predominantly s- or p-type, respectively (see Fig. 5). Hence, the analysis of the metallic case of Section 3.1 applies here, too, i.e.,

$$\mu_{vv'}(\epsilon) \approx eL_\epsilon, \tag{69}$$

where L_ϵ is the extension of the confinement in the direction specified by the unit vector ϵ.

For the interband transition dipole moment, however, the situation is drastically different, since assuming centrosymmetric units cells (this is not strictly the case in semiconductors), making the substitution $\mathbf{r} = \mathbf{R} + \boldsymbol{\rho}$, and setting

$$\int u_e(\boldsymbol{\rho})\epsilon \cdot \boldsymbol{\rho} u_h(\boldsymbol{\rho})\, d\tau = p_{cv}, \tag{70}$$

which in contrast to (59) does not vanish (u_e and u_h have predominantly opposite parities (see Fig. 5b)), one gets

$$\mu_{vv'}(\epsilon) \approx p_{cv} \int F_e^*(\mathbf{r}) F_{hv'}(\mathbf{r})\, d\mathbf{r}, \tag{71}$$

namely $\mu_{vv'}(\epsilon)$ is proportional to the bulk interband transition dipole moment p_{cv} with a proportionality factor equal to the overlap of the electron and hole envelope functions. In particular, for centrosymmetric confinement,

$$\mu_{vv'} \approx p_{cv}\delta_{vv'}; \tag{72}$$

namely, only transitions between a hole and electron state with identical quantum numbers (complete overlap) are allowed, and the transition dipole moment is then equal $p_{cv} \approx ea$, the same as the interband transition dipole moment for the bulk semiconductor. This is an essential characteristic of the interband confinement, and a consequence of the different symmetry properties of the cell periodic parts u_e and u_h of the wavefunction. (see Figs. 5b and 7).

3.2.2. *Level Spacing*

The intraband level spacing, namely that between two electron or two hole states, is the same as in the metallic case, i.e.,

$$\Delta E \approx 1/L^2, \tag{73}$$

but between a hole and an electron state,

$$\Delta E_v = E_g + \frac{\hbar^2 k_v^2}{2m} = E_g + \frac{\hbar^2 \alpha_v^2}{2\mu L^2}, \tag{74}$$

where we have assumed complete overlap, $1/\mu = 1/m_e^* + 1/m_h^*$, and $k_v = \alpha_v/L$ is the quasimomentum related to state v.

3.2.3. *Level Broadening and Lifetime*

One never obtains sharp lines at the frequencies (74) since these are broadened (Fig. 9) by several mechanisms. In quantum confined semiconductor microstructures, the situation concerning the broadening and lifetime of the optical transitions is far more complex than in the metallic case, and this for two main reasons as can be inferred from (73) and (74), namely, superposition of inter- and intraband effects and the nonuniform and noncentrosymmetric electron density distribution. However, we may single out [51] two main broadening mechanisms: the electron–phonon coupling, which introduces homogeneous broadening, and the fluctuations in E_g and L, which introduce an inhomogeneous broadening. The apparent line form and width result from a convolution of the two. Their relative impact can be studied by nonlinear spectroscopic techniques, and in particular with the frequency- or time-resolved hole burning technique [52] or photon echoes.

The electron–phonon coupling in quantum confined semiconductor structures has recently been addressed [53–55] both theoretically and

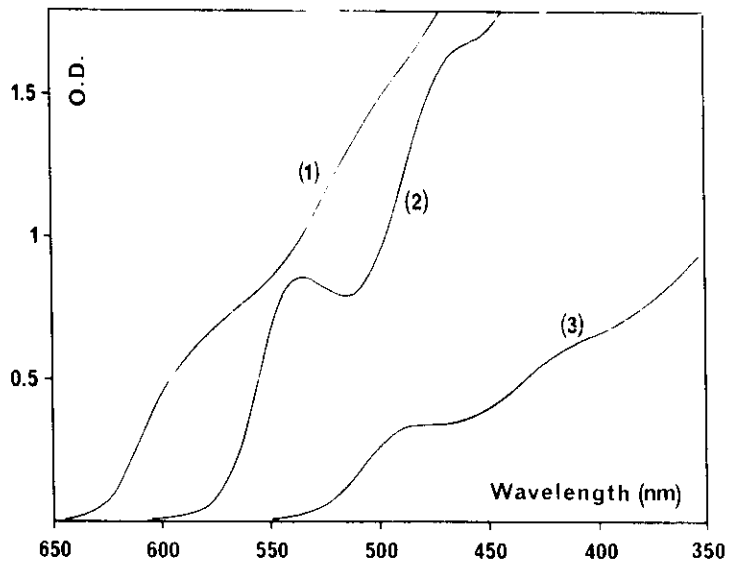

Fig. 9. Absorption spectra for three semiconductor doped glass samples of CdS$_x$Se$_{1-x}$. The mean radii are (1) 6 nm, (2) 2.5 nm, and (3) 1.5 nm (from Ref. 52).

experimentally, and certain aspects are now qualitatively understood. There are three electron–phonon coupling mechanisms:

- the electron–optic polar phonon or Fröhlich coupling;
- the deformation potential;
- the piezoelectric coupling.

All three have been extensively studied for bulk crystals. The electron–optic polar phonon or Fröhlich coupling can be accounted for along the lines of the Huang–Rhys theory [57] and is not expected to be different [53, 56] in the confined microstructures, as the optic phonons are related to intracell polar vibrations and their dispersion over the Brillouin zone is rather flat. In contrast, the deformation potential and eventually the piezoelectric coupling, because of the involvement of acoustic phonons there, may be drastically affected by the quantum confinement. Indeed, the acoustic phonon branches show a very strong dispersion over the Brillouin zone and are therefore sensitive to the quantum confinement. Thus, in the case of a spherical semiconductor crystallite, breathing modes appear, with frequencies $\omega_b \approx v_s/L$, where v_s is the sound velocity, that modulate the electron–hole motion and introduce a broadening that is size and temperature dependent, the latter because of the temperature dependence of the phonon populations. We also point out here that the deformation potential also gives rise [58, 59] to quantum confinement in strained microstructures, and to self-trapping of an electron by an acoustic lattice mode.

To the extent that in quantum confined microstructures one exploits resonantly enhanced optical nonlinearities, the nature of the broadening, whether homogeneous or inhomogeneous, plays an essential role, and several nonlinear spectroscopic techniques have been applied to understand this aspect. The most straightforward ones are the time resolved and spectral hole burning techniques and their variants [52]. There is presently much interest in understanding these broadening mechanisms as they mostly condition the nonlinear optical properties of the quantum confined structures.

3.3. Confinement Potential

As was briefly discussed in Section 2.1, the confinement of the delocalized electron and hole states in a metal or semiconductor is achieved through interfaces with a different material that impedes the motion of charges outside the confined region. In the ideal case, these interfaces are planar to better than an atomic layer if they correspond to natural growth planes. If we disregard the constitution of the substrate, these interfaces in a first approximation can be represented by sharp potential walls of infinite height where the envelope function must vanish. With such a boundary condition, charges are confined

whatever their energy might be, and their level spacing is $\sim L^{-2}$, where L is the extension of the confinement.

In practice, this is never the case and the height must be taken as finite, so that above a certain energy level the charges may move out of the confined region to acceptor states of the surrounding medium. Furthermore, to the extent that the surrounding medium is polarizable and dielectrically responds to fields, the confinement potential cannot be sharp to within an atomic layer but has to be corrected to include the polarization potential and other terms, and therefore acquires a smoother spatial dependence with a range that extends over several unit cells on either side of the interface. Clearly, these additional terms depend on the electronic distribution inside the confined region, and this implies that a self-consistency procedure must be applied to obtain the potential. Such a treatment is in general quite involved, and can be tackled only with highly idealized models where the shape of the confinement is either spherical or consists of parallel planar walls.

The fact that the potential is neither sharp nor of infinite height also complicates the formulation of the boundary conditions for the envelope function, and, as a consequence in the case of the intraband confinement, neither the L^{-2} level spacing law nor the L-dependence of the intraband matrix elements are rigorously obeyed. The interband confinement on the other hand is less sensitive to these aspects, although the selection rules become less strict.

Notwithstanding the previous considerations, an additional complication arise from the potential within the confined region itself, which, as discussed in Section 2.2, consists of the electron–hole Coulomb potential, the many-body interactions, and the potential of the impurities and other defects. Their relative impact depends on the extension of the confinement with respect to the characteristic lengths that were associated to these potential terms and determine their respective strengths. As discussed in Section 2.2, whenever the confinement extension is larger than any of these lengths, the energy spectrum is determined by the corresponding potential term while the confinement only acts as a perturbation on the spectrum. As the confinement extension is reduced below these lengths, however, the roles are inverted and the confinement suppresses the different potential terms and imposes its own spectral distribution. However, the effect of these terms cannot be altogether neglected. Since the variation of these potentials is smooth over distances smaller than the corresponding Bohr radius, to a first approximation their effect can be replaced by that of an equivalent homogeneous electric field, which then leads to a Stark shift of the quantum confined levels. These equivalent electric fields evidently depend on the electronic distribution inside the crystallite, and the problem can only be tackled self-consistently here, too.

The preceding remarks were made both to keep in mind the extreme difficulties related to the solution of the Schrödinger equation (51), either

analytically or numerically, and also to appreciate the importance of even highly idealized potentials that allow one to extract meaningful results. Keeping these remarks in mind, we summarize in the following the most salient features of the simplest potentials that are being used to study the impact of the quantum confinement on the optical properties without undue numerical or analytical effort; these are the quantum well of square and triangular shape (Fig. 10), the quantum wire, and the quantum dot potentials with sharp and infinitely high boundaries. For details, we refer [60] to standard textbooks on quantum mechanics.

3.3.1. Quantum Well

The Schrödinger equation

$$\left[-\frac{\hbar^2}{2m^*}\frac{\partial^2}{\partial z^2}+W(z)\right]\psi(z)=E\psi(z), \tag{75}$$

with $W(z)=0$, for $|z|<L_z/2$, and $=\infty$, for $z\geq L_z/2$, and the boundary condition $\psi(\pm L_z/2)=0$ has the eigenstates

$$\psi_n(z)=\sqrt{\frac{2}{L_z}}\sin k_n z,$$
$$E_n=\frac{\hbar^2}{2m^*}k_n^2=\frac{\hbar^2}{2m^*}\left(\frac{n\pi}{L_z}\right)^2, \qquad n=1,2,\ldots, \tag{76}$$

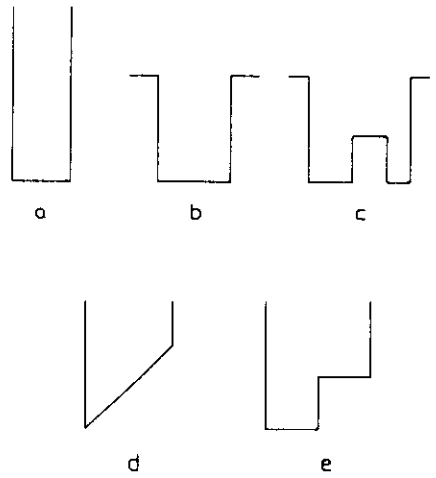

Fig. 10. Five simple quantum wells: (a) infinite square; (b) finite square; (c) double square; (d) triangular; (e) square with a step.

and the transition matrix elements

$$\mu_{nn'}=\frac{16}{\pi^2}\frac{nn'}{(n^2-n'^2)^2}L_z, \qquad \text{for odd } |n-n'|, \tag{77}$$
$$=0, \qquad \text{otherwise.}$$

The Schrödinger equation for finite height symmetric square well potential W can be readily solved. Since it is relevant for strained quantum wells, we give the main results. The eigenstates and eigenenergies are obtained by making the ansatz $\sin kz$ or $\cos kz$ for the wavefunction inside the well, with exponential decay outside. The continuity of the wavefunction and its derivative at the boundary $z=\pm L_z/2$ gives

$$\kappa\tan(kL_z/2)=k, \qquad \text{for even states,}$$
$$\kappa\cot(kL_z/2)=-k, \qquad \text{for odd states.}$$

where

$$k^2=\frac{2m^*E}{\hbar^2}$$

and $\kappa^2=2m^*(E+W)/\hbar^2$. These relations determine k for the even, respectively, odd, parity states and the corresponding eigenenergies from (77). The solutions can be obtained graphically [60]. There is always one bound state. The total number of bound states is

$$n(L_z)=1+\mathrm{Int}\left(\sqrt{\frac{2m^*WL_z^2}{\pi^2\hbar^2}}\right),$$

where $\mathrm{Int}(x)$ denotes the integer part of x.

In connection with the Stark effect, we will also need the solution of the Schrödinger equation for the triangular quantum well

$$\left(-\frac{\hbar^2}{2m^*}\frac{\partial^2}{\partial z^2}+eFz+W\right)\psi(z)=E\psi(z), \tag{78}$$

where W and the boundary conditions are as before. The nonsingular solutions of this equation are the Airy functions

$$\mathrm{Ai}\left[\left(\frac{2mF}{\hbar^2e^2}\right)^{1/3}(eFz-E_n)\right], \tag{79}$$

which oscillate for $z<L/2$, and decay exponentially for $z\to\infty$, where

$$E_n=-(e^2F^2\hbar^2)^{1/3}a_n, \tag{80}$$

where a_n are the zeros of Ai(ξ), which approximately are

$$a_n = -\left[\frac{3\pi}{2}\left(n + \frac{3}{4}\right)\right]^{2/3}. \tag{81}$$

Using these simple potentials, one can proceed to solve more complex cases like the double square well potential (Fig. 10) or the multiple square well potential, and also include tunneling between wells.

3.3.2. *Quantum Wire*

For a rectangular cross section, the Schrödinger equation is

$$\left[-\frac{\hbar^2}{2m_x^*}\frac{\partial^2}{\partial x^2} - \frac{\hbar^2}{2m_y^*}\frac{\partial^2}{\partial y^2} + W(x,y)\right]\psi(x,y) = E\psi(x,y), \tag{82}$$

with $W(x,y) = 0$, for $|x| < L_x/2$ and $|y| < L_y/2$, and $= \infty$ outside this region. This is separable to two equations, each of the form (75), and the solutions then are simply

$$\psi_{nm}(x,y) = \psi_n(x)\psi_m(y),$$
$$E_{nm} = E_n + E_m. \tag{83}$$

For a circular cross section with $m_x^* = m_y^* = m^*$, the Schrödinger potential well is $W(x,y) = 0$, for $x^2 + y^2 < (L/2)^2$, and $= \infty$ outside this region. After transforming to cylindrical coordinates ρ and ϕ, one finds

$$\psi_{nm}(\rho,\phi) = \left(\frac{8}{L^2}\right)^{1/2}\frac{1}{J_{n+1}(\alpha_n)}J_n\left(\alpha_n\frac{2\rho}{L}\right)e^{im\phi}, \tag{84}$$

$$E_n = \frac{\hbar^2 k_n^2}{2m^*}, \tag{85}$$

where $k_n = 2\alpha_n/L$ is fixed by the boundary condition

$$J_n(k_n L/2) = 0. \tag{86}$$

Because Bessel functions asymptotically approach trigonometric ones, we expect a correspondence for large n between states (83) and (85) when $L_x = L_y$.

3.3.3. *Quantum Dot*

The Schrödinger equation for a quantum parallepiped of lengths L_x, L_y, and L_z is readily solved since it is separable into three equations, each of the form (75). The spectrum presents degeneracies whenever the three lengths L_x, L_y, and L_z are rational numbers, and are in particular threefold degenerate for a quantum cube ($L_x = L_y = L_z$). Of particular interest is the spherical

quantum dot with $m_x^* = m_y^* = m_z^* = m^*$ and

$$W(x,y,z) = 0, \qquad \text{for } x^2 + y^2 + z^2 < (L/2)^2,$$
$$= \infty, \qquad \text{outside this region.}$$

After transforming to spherical coordinates r, θ, ϕ, the Schrödinger equation can be solved in terms of Bessel functions and spherical harmonics:

$$\psi_{nlm}(r,\theta,\phi) = \left(\frac{16}{L^3}\right)^{1/2}\frac{1}{J_{l+1}(\alpha_{nl})}J_l\left(\alpha_{nl}\frac{2r}{L}\right)Y_l^m(\theta,\phi). \tag{87}$$

Putting $E_0 = \hbar^2/2mL^2$ and $k_{nl} = 2\alpha_{nl}/L$, the eigenenergies are

$$E_{nlm} = (\alpha_{nl})^2 E_0 = \hbar^2 k_{nl}^2/2m^*, \tag{88}$$

where k_{nl} is the quasimomentum defined by the boundary condition

$$J_{l+1}(k_{nl}L/2) = 0, \tag{89}$$

and the orbital and angular numbers, n and l, respectively, can vary independently of each other with $n = 0, 1, \ldots$, and $l = 1, 2, \ldots$, the azimuthal number $|m| = 0, 1, 2, \ldots, l$; the states (88) thus have a $(2l + 1)$-fold degeneracy. Here again, because of the asymptotic correspondence between trigonometric and Bessel functions, we expect the spectra of a quantum cube and a sphere to correspond to each other.

The intraband transition dipole moment is

$$\langle nlm|\mu|n'l'm'\rangle = \frac{2LE_0(E_rE_s)^{1/2}}{(E_r - E_s)}A_{mm'}, \tag{90}$$

where $r = nl$ and $s = n'l'$ with $|l - l'| = 1$ and $m = m'$, $m' \pm 1$. It is easy to check from the previous expressions of the energy levels that the energy spacing for allowed transitions obeys the law

$$\Delta E_{rs} \sim 1/L^2, \tag{91}$$

and the intraband matrix elements $\sim L$ as expected for intraband confinement.

In contrast, for interband transitions, the dipole moment element is

$$\langle enlm|\mu|hn'l'm'\rangle \approx p_{cv}\delta_{nn'}\delta_{ll'}\delta_{mm'}, \tag{92}$$

and the energy spacing is

$$\Delta E = E_g + \frac{\hbar^2 k_n^2}{2\mu} = E_g + \frac{\hbar^2}{2\mu}\left(\frac{2\alpha_n^2}{L}\right), \tag{93}$$

as expected for interband confinement.

The preceding results using simple confinement potentials allow one to grasp the salient features of the quantum confinement and the way it affects the optical transitions. Clearly, its main effect is a spectral condensation where the widely and continuously spread transition energies in the bulk change to a series of discrete states. Since the electron density is unaffected, this implies that a much larger number of electrons participate in the allowed transitions between these discrete states in the confined system than in the same energy range in the bulk.

In Fig. 3, we show how the density of states of a bulk isotropic semiconductor, close to its gap E_0, is modified as it is successively subject to one-, two-, and three-dimensional confinement.

3.3.4. Strain Confinement

We give here a simple description [58] of the confinement through local deformation or strain. Suppose that a crystal lattice is deformed, producing a dilation $\Delta(\mathbf{r})$ over a localized region, and let us denote by $\mathbf{x}(\mathbf{r})$ the displacement of a small quantity of matter at the point $\mathbf{r}$, so that

$$\Delta(\mathbf{r}) = \nabla \cdot \mathbf{x}(\mathbf{r}).$$

Then, an electron (or a hole) at the bottom (top) of the band feels a perturbing potential [61]

$$V(\mathbf{r}) = E_d \Delta(\mathbf{r}),$$

where E_d is the deformation potential constant. Let us for simplicity assume that

$$\Delta(r) = \Delta, \qquad \text{for } r \le R,$$
$$= 0, \qquad \text{for } r > R.$$

Then, the elastic potential energy is given by

$$v = \left(\frac{4}{3}\pi R^3\right)\left(\frac{1}{2}C\Delta^2\right) \equiv \frac{\hbar^2}{2m}\frac{\delta^2}{R_0 R},$$

where C is an effective elastic constant, $R_0 = 3mE_d^2/\pi\hbar^2 C$, and

$$\delta = \frac{2m}{\hbar^2} R^2 E_d \Delta.$$

The condition for a bound state in the potential well is $\delta > (\pi/2)^2$, if $E_d\Delta$ is negative, and the binding energy is

$$E = \frac{\hbar^2}{2mR^2}(\zeta \cot \zeta)^2,$$

where ζ is determined by

$$(\zeta/\sin\zeta)^2 = \delta, \qquad \pi/2 < \zeta < \pi.$$

From the preceding considerations, one can see that local strain leads to localization and confinement. Clearly, this confinement can exist with the confinement brought about by interfaces, as previously discussed, and can also introduce additional states or level displacements and broadening. Since most quantum confined microstructures are alloys of the type AB_xC_{1-x}, where $0 \le x \le 1$, one may also have localization and confinement because of local fluctuations of x. This problem can be treated [59] along the same lines as the strain.

4. THE IMPACT OF QUANTUM CONFINEMENT ON OPTICAL NONLINEARITIES: NONRESONANT CASE

The quantum confinement acts on all characteristics of an optical transition: oscillator strength, selection rules, level spacing, broadening, and lifetime. Here and in the following section, we wish to assess the compound effect that these changes have on the optical nonlinearities. As stated in the introduction, we will concentrate our attention on the cubic optical nonlinearities and in particular on the resonant and nonresonant optical Kerr effect, which we recall is also defined as the light induced changes in the index of refraction and absorption. We will complete this discussion with some remarks on the second-order susceptibilities as well, which are conditioned by the asymmetry of the intracell charge density distribution, a characteristic that is not directly affected by the quantum confinement. To be more precise in the following, we shall first discuss the impact of dimensionality on the cubic nonlinearity $\chi^{(3)}$ as this is reflected in the critical regions of the joint density of states. We will see that these lead to scaling laws for the cubic and higher odd order susceptibilities. The impact of the quantum confinement on the optical Kerr effect and related parametric effects will be subsequently discussed in two specific cases, the linear chains and the quantum dots. Both cases concern global confinement where one can single out the size effects brought about by confinement without any reference to a precise potential and bulk behavior. We will see that the inter- and intraband quantum confinement act in a quite distinct way. We also briefly discuss the modifications that arise from coupling of two or more quantum confined microstructures.

4.1. Dimensionality Effects and Scaling Laws

As was stressed in Section 2, see (45), (46), and (47), the susceptibilities in the transparency region are expressed as integrals over the Brillouin zone, and the

main contribution to these integrals is expected to come from the critical regions in the joint density of states. Since the signature of the latter is directly related to the dimensionality of the electron charge density, this establishes [47] a relation between the optical susceptibilities $\chi^{(2n+1)}$ and the topology and dimensionality of the joint density of states, and in particular allows one to express these nonlinearities in terms of the values of Ω_{vc} and ω_{cv} at these critical regions only, and derive scaling laws. In contrast, the second-order susceptibility $\chi^{(2)}$ is not sensitive to these critical regions in **k** space but rather to the overall joint density of states, since $\chi^{(2)}$ is determined by a local property, namely the asymmetry of the intracell charge density distribution. We will summarize the salient results of this discussion since the details can be found elsewhere [47, 62], and concentrate our attention on the nonresonant case only. Since the critical regions in a given system are well separated from each other, one may assume that their effect is additive and consider the contribution for each one separately.

One-dimensional system with critical point E_0. One finds [44]

$$\chi^{(3)} = \chi_a^{(3)}\left(\frac{E_F}{E_0}\right)^6 \tag{94a}$$

and, more generally,

$$\chi^{(2n-1)} = \chi_a^{(2n-1)}\left(\frac{E_F}{E_0}\right)^{4n-2} \tag{94b}$$

where $\chi_a^{(2n-1)}/v_0$ is the $(2n-1)$th order polarizability of an isolated unit cell. The crucial quantity here is the delocalization length

$$L_d = a\frac{E_F}{E_0} = aN_d. \tag{95}$$

Expressions (94a and b) are valid when $E_F/E_0 \gg 1$, which corresponds to very dispersive bands or very delocalized electrons. If such is the case, a careful analysis of (46) shows that the first term inside the integral, also called the intraband or Franz–Keldysh term, is the dominant term, and this leads to $\chi^{(3)} > 0$. For flat bands or localized electrons ($N_d \approx 1$) the second term, also called the interband or Stark term, becomes dominant, and $\chi^{(3)} < 0$.

Two-dimensional system with critical line E_1. One finds [47, 62]

$$\chi^{(3)} \approx p_{cv}^2 E_1^5 \tag{96a}$$

and, in general,

$$\chi^{(2n-1)} \approx p_{cv}^2 E_1^{3n-1}. \tag{96b}$$

Three-dimensional system with critical surface E_2. One finds [47, 62]

$$\chi^{(3)} \approx P_{cv}^2/E_2^{9/2} \tag{97a}$$

and, in general,

$$\chi^{(2n-1)} \approx P_{cv}^2/E_2^{2n+1/2}. \tag{97b}$$

The preceding results are valid for frequencies ω well below the onset of electronic transitions. For frequencies not too close to the gap energies E_0, E_1, or E_2, one can still use the previous expressions and expressions (9a,b,c) for the joint density of states simply by replacing E_i by $\tilde{E}_i = E_i - \hbar\omega$. Close to the critical regions, the expressions break down as the behavior is dominated by the dynamics of the resonance there and other characteristics of the transition, and each case must be examined separately.

We wish to complete this discussion with a comment concerning the second-order susceptibility $\chi^{(2)}$. In this quantity, the inter- and intraband terms in (47) can have either sign so that they may add or substract inside the integral. Careful analysis of Eq. (47) reveals [44, 47] that contributions to the integral only come from regions where Ω_{vc} is a complex number. The integrand vanishes whenever Ω_{vc} becomes either only real or pure imaginary, and this is precisely what happens at the edge of the Brillouin zone where the critical points occur. Thus, in constrast to $\chi^{(3)}$, $\chi^{(2)}$ does not take full advantage of the infinite density of states at the critical points and the highly delocalized character of the states there. In particular, the critical point analysis and the derivation of scaling laws is not as straightforward as for $\chi^{(3)}$.

4.2. Size Effects in Conjugated Chains

We shall discuss here the case of the optical nonlinearities of finite conjugated chains, and see how size effects are brought in by quantum confinement. We shall explicitly consider chains with and without bond alternation. With some simplifying assumptions concerning the electronic distribution [44, 63], one can use a fully analytical treatment and gain some insight into the impact of the quantum confinement. Despite the very idealized picture we will use here, the general conclusions are of interest in ongoing research activity on nonlinear organic materials, and deserve some attention.

4.2.1. Chains without Bond Alternation

We use the Hückel approximation [63, 64] and write the wave function as $\psi = \sum_n c_n \phi_n$ where ϕ_n is the atomic orbital on atom n and the coefficients c_n for a finite chain with $2N$ equally spaced atoms in the presence of an electric

field E are determined through

$$c_n(-\epsilon + nw) + \beta(c_{n-1} + c_{n+1}) = 0, \tag{98}$$

where β is the resonance (hopping) energy between neighboring atoms, the energy ϵ is determined through the boundary conditions $c_0 = c_{2N+1} = 0$, and $w = eaE$, where a is the interatomic distance (unit cell length). The solution of (98) is

$$c_n = AJ_{n-\epsilon/w}(-2w/\beta) + BY_{n-\epsilon/w}(-2w/\beta) = 0, \tag{99}$$

where J_ν and Y_ν are the Bessel and Von Newman functions. From the boundary condition $c_0 = c_{2N+1} = 0$, one gets

$$J_{-\gamma\xi}(2\gamma)Y_{1-\gamma\xi}(2\bar{\gamma}) - J_{\bar{\gamma}/\bar{\gamma}-\gamma\xi}Y_{-\gamma\xi}(2\gamma) = 0, \tag{100}$$

where $\gamma = -\beta/w$, $\xi = -\delta/\beta$, and $\bar{\gamma} = (N+1)\gamma$. The roots of this equation give the $2N$ eigenvalues ϵ_n.

For zero electric field $E = 0$, the roots reduce to

$$\epsilon_n^0 = 2\beta\cos\theta_n^0, \qquad \theta_n^0 = \frac{n\pi}{N+1}, \quad n = 1, 2, \ldots, N, \tag{101}$$

while at the high field intensity limit ($\gamma \ll 1$) one obtains the Stark ladder [65, 66] spectrum

$$\epsilon_n = n\omega = naE, \tag{102}$$

and the same is true for intermediate field intensities ($\bar{\gamma} \ll 1$ but $\gamma \gg 1$). For low field intensities where perturbation theory can be used, namely $\gamma \gg 1$ and $\bar{\gamma} \gg 1$, using the double asymptotic development of Bessel functions and rearranging the expressions, one obtains [44], for the total energy of the electron system,

$$W = \sum_{n=1}^{\infty} \epsilon_n = W_0 - N\beta \sum_{n=0}^{\infty} \frac{\lambda^{(k)}}{\bar{\gamma}^{2k}}, \tag{103}$$

where the $\lambda^{(k)}$s are constants that in principle can be calculated. Inserting $\bar{\gamma} = -(N+1)\beta/eaE$, using the definition of the polarizabilities for a symmetric molecule,

$$W = W_0 - \sum_{n=1}^{\infty} -\frac{1}{2k-1}\alpha^{(2k-1)}E^{2k-1}, \tag{104}$$

and identifying terms of the same order in E in Eqs. (103) and (104), one obtains

$$\alpha^{(2n-1)} \approx N^{2n+1}e^{2n}a^{2n}/\beta^{2n-1} = L^{2n+1}e^{2n}/a\beta^{2n-1}, \tag{105}$$

which is valid for $N \gg 1$; $L = Na$ is the half length of the chain. In particular, for the linear and third-order polarizabilities one has

$$\alpha \sim N^3e^2a^2/\beta = L^3e^2/a\beta, \tag{106a}$$

$$\gamma \sim N^5e^4a^4/\beta = L^5e^4/a\beta^3, \tag{106b}$$

respectively, results that were also obtained [67] by directly calculating (42a) and (42c) with the matrix elements and energy levels of the free-electron model in a box [68, 69] with infinite potential walls (see Section 3.3). This is clearly a size-dependent effect brought about by intraband confinement.

In order to place this in the proper context, let us also write down the results for the infinite chain. Without bond alternation, one has

$$\epsilon(k) = 2\beta\cos ka, \tag{107}$$

where k varies over all values within the interval $[0, \pi/a]$ (Brillouin zone). From a development for $ka < 1$, one obtains [70] the effective mass

$$m^* = \frac{\hbar^2}{2\beta a^2}. \tag{108}$$

Thus, we see that the discrete states (101) of the finite chain fall exactly on the bands (107), and are only those that have nodes at the chain ends. This precisely excludes the end points 0 and π/a of the band and their neighborhood (see Fig. 11). As a consequence, the two extreme levels of the discrete spectrum (101) are shifted above and below, respectively, the band end points by an amount that is precisely the characteristics confinement energy $\hbar^2\pi^2/2L^2m^*$. A simple calculation of (101) for $\theta_n < 1$ shows that the discrete spectrum can be written as

$$E_n = \frac{\hbar^2}{2m^*}\left(\frac{\pi n}{L}\right)^2,$$

precisely the same as for a free particle in a box with effective mass m^*. We notice that the latter strongly depends on β, and this parameter measures the delocalization ability of the electrons along the chain and also determines the band width. The transition dipole moments are clearly only intraband ones as given by (77), and their introduction in (42) together with (76) lead to expressions (106a) and (106b).

4.2.2. *Chains with Bond Alternation*

The chain with bond alternation is related to the chain without bond alternation by a Peierls-type phase transition. One introduces [63, 44] two resonance energies β_1 and β_2 to characterize bond alternation, and one finds that for the infinite chain the energy spectrum consists of two bands that are mirror images to each other, the valence (hole) and conduction (electron)

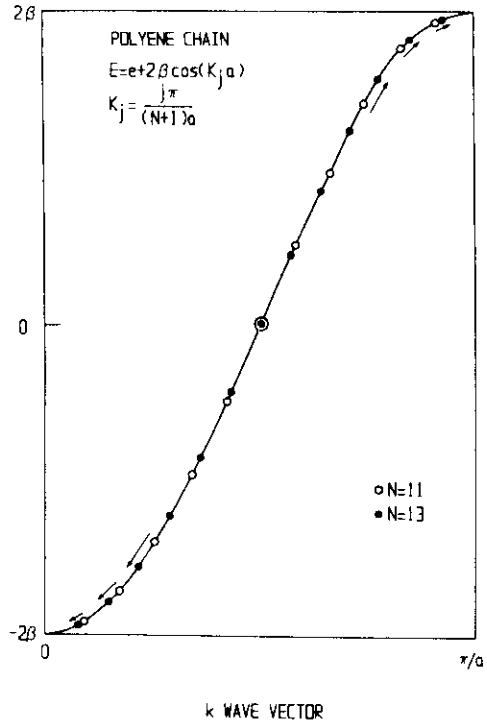

Fig. 11. A schematic view of the quantum confinement in a one-dimensional chain without bond alternation (from Ref. 70).

bands, with respect to the Fermi level $E_F = \beta_1 + \beta_2$, which coincides with the total half width of the band. The minimum separation of the two bands, or band gap E_g, is an E_0-type critical point where the joint density of states becomes infinite according to (10). Analytically, one has [44]

$$E_{c,v}(k) = \pm\beta_2\sqrt{1 + v^2 + 2v\cos ka} \equiv \pm\beta_2\xi_0 \tag{109}$$

for the two bands with effective masses [71]

$$m_e^* = m_h^* = \left(\frac{1}{\beta_1} + \frac{1}{\beta_2}\right)\frac{\hbar^2}{a^2}, \tag{110}$$

$$E_g = E_0 = 2|\beta_1 - \beta_2| \tag{111}$$

for the gap and

$$e\Omega_{cv} = ea(1 - v^2)^2/4\xi_0^2 \tag{112}$$

for the transition dipole moment, which reaches its largest value at $ka = \pi$:

$$e|\Omega_{cv}(\pi)| = a\frac{\beta_1 + \beta_2}{\beta_1 - \beta_2} = \frac{1}{2}ea\frac{E_F}{E_g} = eL_d \tag{113}$$

where L_d was defined in (95). The critical point E_0 at $ka = \pi$ thus plays a crucial role; it is the point where the valence and conduction states respectively reduce to bonding and antibonding molecular states within each unit cell. It is worthwhile noticing by going over to the Jones zone that this critical point plays a pivotal role, and is the only one that preserves a metal-like character in the Peierls transition.

As we go over the finite bond alternated chain of length $L = Na$, the quantum confinement starts excluding states from the band extremes, and precisely from the part of spectrum where the critical point is located since the molecular orbitals must possess at least two nodes at the chain ends. As long as $4L_d < L$, these changes are minor and most states are still accumulated there. This part of the band being relatively flat, however, as a consequence, the optical properties and the nonlinear ones in particular are not affected, and one finds [63] that, for $4L_d < L$,

$$\chi^{(3)} \sim N_d^6 \sim L_d^6, \tag{114}$$

namely the same dependence on N_d(or L_d) as for the infinite chain, which also implies that any defects along a chain more distant than $4L_d$ apart have no effect on the behavior of the optical Kerr effect.

However, as L becomes comparable to L_d, a dramatic change occurs in the spectrum since the average state spacing now is of the order of E_c in (15), namely of the order of $|\beta_1 - \beta_2|$, and the singular behavior of the energy region around the ghost of the energy gap of the infinite chain is suppressed for $4L_d \geq L$. Actually, for $4L_d \geq L$ one obtains a free-electron behavior in a box of length L. Indeed, the L_d^6-law (114) breaks down, and one recovers the L^5-dependence (106b) characteristic of a chain without bond alternation.

It is worthwhile also to notice that the two terms in (46), the Franz–Keldysh and Stark terms, have their counterparts in the two terms in (42c) if the occupation of the states is properly taken into account. From this analogy, one may say that even a molecule or an atom with more than two energy levels has Franz–Keldysh and Stark energy shifts related to the first and second terms in (42c), respectively, and the sign of γ is determined by the relative magnitude of these two shifts in a way similar to that discussed for the infinite system.

To summarize the previous discussion, the nonresonant optical nonlinearities show size-dependent effects brought in by quantum confinement only when all involved virtual optical transitions are intraband. The resonant optical nonlinearities, on the other hand, must be discussed by taking proper consideration of the broadening and lifetime in the involved resonances. This

will be exemplified in the following in the case of semiconductor spherical crystallites of size smaller than the electron radius, also called semiconductor quantum dots.

5. IMPACT OF QUANTUM CONFINEMENT ON OPTICAL NONLINEARITIES: RESONANT CASE

As was stated in the introduction, we shall mainly be concerned with the resonant optical Kerr effect and its related parametric effect, the electroabsorption. This is because in this effect one can exploit a multiple resonant behavior in a very narrow frequency region. We shall concentrate our attention only on spherical quantum confined crystallities, and we shall distinguish the metal and semiconductor cases as they roughly correspond to the intraband and interband confinement cases, respectively.

5.1. Optical Kerr Effect in Quantum Dots: Metal and Semiconductor Crystallites

We now wish to discuss [13] the resonant optical nonlinearities of quantum confined metal and semiconductor spherical crystallites. There are two main reasons for the present interest on these systems. First, the confinement here is imposed isotropically in all three dimensions; hence, the behavior of their optical properties can be more naturally contrasted with that of the usually optically isotropic bulk metal or semiconductor crystal. Second, these crystallites when embedded in a transparent dielectric constitute a class of composite materials that have potential applications for optoelectronic devices, and therefore are of certain technological interest. In order to give a qualitative as well as a quantitative presentation of the effects related to the confinement, we will introduce some drastic simplifications regarding these composites, which have already formed the basis of our discussion of the dielectric confinement (see also Fig. 4).

These metal or semiconductor crystallites are uniformly and randomly distributed in small volume concentration in a transparent dielectric, solid or liquid, which will be assumed to be an ideal isotropic medium of dielectric constant ϵ_0, a scalar that shows no resonances and hence no absorption or dispersion in the frequency range of interest. The crystallites will be assumed spherical in shape with a diameter L that is much smaller than both the optical wavelength λ and the interparticle distance, so that mutual interactions can be neglected. These assumptions formed the basis of our discussion of the dielectric confinement (Section 2.3), and it was shown that this is quite distinct from the quantum confinement. Furthermore, the dielectric confinement turns out to be important for the metal composites but much less so for the

semiconductor ones. Here, we concentrate our attention on the quantum confinement effects and discuss separately the metal and semiconductor cases to illustrate the two quantum confinement types, the intra- and interband, respectively.

In contrast, however, to the case of the dielectric confinement discussed in Section 2.3, here the size distribution of the particles affects the behavior of the optical properties, and in particular the nonlinear ones since it introduces a spread in the level spacings that leads to an inhomogeneous broadening [13, 51, 55] in the transitions in addition to the homogeneous one, which usually arises from electron–phonon coupling. We recall [13] that these particles are grown inside the dielectric matrix by a more or less thermally controlled diffusion process, and to a first approximation their average size is L, and their size distribution around this average value can be derived with the help of the Lifshitz–Slezhov model [72]

$$\bar{L} = \left(\frac{4}{9}\sigma D c \tau\right)^{1/3}, \tag{115}$$

$$P(u) = \frac{3^4 e}{2^{5/3}} \frac{u^2 e^{-1/(1-2u/3)}}{(u+3)^{7/3}(\frac{3}{2}-u)^{11/3}}, \qquad u < 1.5, \tag{116}$$

$$= 0, \qquad u \geq 1.5,$$

where $u = L/\bar{L}$; it is an asymmetric distribution with faster fall-off for $L > \bar{L}$.

Our concern here is the optimally resonant optical Kerr effect susceptibility $\chi^{(3)}(\omega, -\omega, \omega)$, and more generally $\chi^{(3)}(\omega, -\omega', \omega')$ where ω and ω' are close to resonances. We shall also discuss the limiting case of $\omega' \to 0$, which is a parametric process.

5.1.1. *Metal Quantum Dots. Intraband Confinement*

In an ideal metal with a single half-filled band formed from s wavefunctions, $u_e(r) = u_s(r) \approx 1$ and $m_e^* = m_h^* \approx m$, and the electron and hole wavefunctions are identical and coincide with the envelope wavefunctions. The wavefunctions and energy spectrum were given in Section 3.3.3. For $n \gg 1$, the roots of (89) can be simplified by

$$\alpha_{nl} = (2n + l)\pi/2,$$

and when a density of states can be defined, it is given by the bulk value

$$\nu(E) = \frac{V}{2\pi^2}\left(\frac{2m}{\hbar^2}\right)^{3/2} E^{1/2} = \frac{2}{3\pi}\frac{E^{1/2}}{E_0^{3/2}},$$

including spin degeneracy, where V is the volume of the spherical crystallites.

The energy spacing between two states, the one of energy E, connected by a dipole allowed transition is

$$\Delta E = \pi(EE_0)^{1/2}.$$

If we assign the same value to all states between E and $E + \Delta E$, their number is

$$N(E) = v(E)\Delta E = \frac{2E}{3E_0},$$

and the Fermi level E_F is independent on the crystallite size:

$$E_F = \frac{\hbar^2}{2m}\left(3\pi^2 \frac{N}{V}\right)^{2/3}.$$

The intraband transition dipole moment between states $r = nlm$ and $s = n'l'm'$, where $|l - l'| = 1$, is

$$\pi_{rs} = \frac{2LeE_0}{i\hbar} \frac{(E_r E_s)^{1/2}}{E_s - E_r} A_{mm'},$$

where $A_{mm'}$ is an angular factor. Finally, we associate two relaxation times T_2 and T_1, the coherence and energy relaxation times, respectively, the same for all transitions.

With these preliminaries, one gets from (37) [38, 73, 74],

$$\chi^{(1)}(\omega) = \frac{\alpha(\omega)}{V} = \frac{\Omega_p^2}{4\pi(\omega + iT_2^{-1})^2} - \frac{2A_2}{\hbar\omega^2} \sum_{r,s} \rho_{rr}^{(0)} |\pi_{rs}^e|^2 \frac{\omega_{rs}}{\omega_{rs}^2 + (\omega + iT_2^{-1})^2} \tag{117}$$

for the linear susceptibility, where Ω_p is the plasma frequency, $\Omega_p^2 = 4\pi Ne^2/mV$, and $A_2 \approx 1/3$ for $l \gg 1$. The first term is the bare Drude term, the same as for the bulk if we disregard the small term T_2^{-2} in the denominator (compare with (48)). In the second term in (117), taking into consideration (90), we expect that the main contribution comes from transitions with $\omega_{rs} = 0$ or $\omega_{rs} = \omega$. The first case amounts to a small correction in the real part of the Drude term, which actually renormalizes the plasma frequency, while the second case, after reverting to an integration over the density of states and then using the identity $1/(x + i\Gamma) \to P(1/x) - i\pi\delta(x)$ when $\Gamma \to 0$, reads

$$\chi(\omega) = i\frac{\Omega_p^2}{4\pi\omega^3} \frac{v_F}{\chi} g_3(v), \tag{118}$$

where $g_3(v)$ is given by (65). This term lumped together with the first term in (117) again gives a Drude term with mean collision time τ_{eff} that takes into account the encounters of the electrons with the surface as well. In the large sphere limit, τ_{eff} reduces to $\tau_b = T_2/2$. The important point to remember is that $\chi^{(1)}(\omega)$ is essentially size-independent, and this also comports with our previous assumption in connection with the dielectric confinement (Section 2.3) that ϵ_V defined by (16) can be identified with the bulk dielectric constant.

The resonant third-order susceptibility is calculated [38, 73] for (42c) by inserting the expressions for π_{rs} and ΔE_{rs} derived in the preceding. One gets

$$\chi^{(3)}(\omega, -\omega, \omega) = -i\frac{64}{45\pi^2} T_1 T_2 \frac{2}{L^3} \frac{e^4}{m^2\hbar^5\omega^7} E_F^4 g_1(v)\left(1 - \frac{a}{a_0}\right), \tag{119}$$

with a_0 given by

$$a_0 = T_2(2E_F/m)^{1/2} g_1(v)/[g_2(v) + g_3(v)],$$

where $g_1(v)$, $g_2(v)$, and $g_3(v)$, like $g_s(v)$ in (65), are numbers of order 1. The important point to notice in (119) is that $\chi^{(3)}$ is negative imaginary and size-dependent, $\chi^{(3)} \approx 1/L^3$ for $a < a_0$. Actually, this term rigorously vanishes for the bulk metal since it results from electric dipole transition. We recall [7] that in the bulk metal $\chi^{(3)}$ results from the magnetic part of the Lorentz force in the equation of intraband motion of the electron, while the electric dipole contribution is zero.

The experimental results [74] actually never showed such a size dependence in $\chi^{(3)}$. The reason is that the intraband contribution in actual metal crystallites is not the sole polarization mechanism. Two more mechanisms contribute there with quite distinctively different behavior that dominates that of the intraband term. One mechanism is an interband term that arises from electronic dipole transitions between the filled d band states and the empty quantum confined ones in the s–p band, and gives a contribution that is negative imaginary but size-independent since the d-electrons are unaffected by the confinement. The other mechanism is the hot electron contribution that results from the modification of the populations of the electron states, the Fermi - Dirac distribution, caused by the elevation of their temperature subsequent to the absorption of photons in the resonant process, but before the heat is released to the lattice of the crystallite; this leads to a contribution to $\chi^{(3)}$ that is positive imaginary and size-independent. A careful analysis [44, 74] of the optical Kerr coefficient using the the optical conjugation technique clearly showed that the third mechanism is the dominant one, and also that even the interband term is larger than the intraband one.

Thus, intraband confinement leads to a characteristic size-dependent term in the optical Kerr susceptibility, while it roughly leaves unaffected the linear susceptibility. However, this contribution to $\chi^{(3)}$ in real metal quantum dots is dominated by other contributions, and cannot be experimentally demonstrated.

5.1.2. *Semiconductor Quantum Dots: Interband Confinement*

The ground state of the quantum confined semiconductor crystallite being the empty hole and electron state, the optical nonlinearity will result from the creation of electron–hole pairs by interband photoexcitation and the subsequent interaction of this pair with different perturbations inside the quantum confined crystallite.

For semiconductor crystallites, the situation is far more complex than for the metallic ones, and this resides in the complexity of the interaction terms in the Schrödinger equation (51), which are only partially screened. They are the electron–hole interaction, the many-body interactions, which also include the electron–hole pair–hair interactions that lead to biexciton formation in the bulk, and the electron/hole–impurity interaction. These interactions can introduce drastic modifications in the spectrum of the quantum confined crystallite and its optical characteristics, and accordingly modify the optical nonlinearities [75, 77]. If we assimilate these interactions by those of equivalent fields, these modifications will result from three causes:

- level shifts;
- breakdown of selection rules and appearance of new allowed transitions;
- redistribution of oscillator strengths;

and will affect the optimal resonant behavior of the third-order susceptibility $\chi^{(3)}(\omega, -\omega', \omega')$.

We concentrate our attention on the $1s$–$1s$ quantum confined transition and designate by ω_{1s} the transition frequency, so that

$$\hbar\omega_{1s} = E_g + \frac{\hbar\pi^2}{2\mu L^2}, \tag{120}$$

where $1/\mu = 1/m_e^* + 1/m_h^*$, and we have neglected any corrections from polarization interactions. To the extent that this transition may be more or less modified by the different terms in the Schrödinger equation [51], we may distinguish [13] three types of nonlinearities.

Saturation nonlinearity [51]. If the electron and hole motions are completely decoupled and the selection rules (92) rigorously apply, then the $1s$–$1s$ transition is isolated enough and each crystallite behaves as an ideal two-level system that may be bleached at the same frequency ω that is resonant with ω_{1s}, and thus contribute to the degenerate optical Kerr susceptibility $\chi^{(3)}(\omega, -\omega, \omega)$.

Coulomb interaction mediated nonlinearity [75–78]. If electron–hole pair–pair Coulomb and exchange interaction is important, then an electron–hole pair created by resonant photoexcitation at $\omega \approx \omega_{1s}$ will shift the transition frequency for resonant photoexcitation of a second electron–hole pair to a new frequency ω'_{1s} or, otherwise stated, in the presence of Coulomb interactions, transitions between one-pair and two-pair states lead to induced absorption at a frequency different from $\omega \approx \omega_{1s}$.

Impurity dominated nonlinearity [79]. If the photocreated electron and hole are rapidly trapped by surface defects of the crystallite, they set up static electric fields that shift the quantum confined levels, inducing absorption in new frequencies ω' so that the optimally resonant Kerr effect susceptibility is $\chi^{(3)}(\omega', -\omega, \omega)$. It is difficult at the present stage of our knowledge to give numbers for such a mechanism, and we shall not discuss it any further except to point out that this mechanism can be time resolved from the two previous ones since it takes time for the electron or hole to be trapped.

Let us consider [80, 81] the first case, and restrict ourseleves to the $1s$–$1s$ transition. The relevant degenerate third-order susceptibility $\chi^{(3)}(\omega, -\omega, \omega)$, with $\omega \approx \omega_s$, can be easily calculated from (36) using the interband transition dipole moment matrix element (72) and introducing the coherence and energy relaxation times T_2 and T_1, respectively. Since the system actually behaves as a two-level system, we may also use the analytical treatment of a two-level system in an intense optical field of frequency ω and arbitrary intensity I to obtain [80]

$$\chi(\omega, I) = \frac{\alpha(\omega, I)}{V} = \frac{1}{V}\left|\frac{ep_{cv}}{m\omega}\right|^2 \frac{1}{\hbar} \frac{1}{\omega_{1s} - \omega - i/T_2} \frac{1 + (\omega_{1s} - \omega)^2 T_2^2}{1 + (\omega_{1s} - \omega)^2 T_2^2 + I/I_s}, \tag{121}$$

where

$$I_s = \left|\frac{m\omega\hbar}{ep_{cv}}\right|^2 \frac{nc}{8\pi T_1 T_2},$$

which also shows the saturation regime anticipated in the preceding. At low intensity, a Taylor expansion around $I \approx 0$ gives the desired optical Kerr coefficient of crystallite of volume V and extension L:

$$\chi_L^{(3)}(\omega, -\omega, \omega) = \frac{1}{V\hbar^3}\left|\frac{ep_{cv}}{\omega}\right|^4 \frac{T_1 T_2^2}{\omega_{1s} - \omega - i/T_2} \frac{1}{1 + (\omega_{1s} - \omega)^2 T_2^2}, \tag{122}$$

while for the linear susceptibility,

$$\chi^{(1)}(\omega) = \frac{1}{V\hbar}\left|\frac{ep_{cv}}{m\omega}\right|^2 \frac{1}{\omega_{1s} - \omega - i/T_2}. \tag{123}$$

Taking the size distribution in actual composites into account, one gets

$$\chi^{(3)}(\omega, -\omega, \omega) = \int_{-\infty}^{\infty} \chi_L^{(3)}(\omega, -\omega, \omega) f(L)\, d\ln L, \tag{124}$$

and similarly for the absorption coefficient.

From (122) and (123), one can easily derive the expression for the figure of merit,

$$\frac{\chi^{(3)}}{\alpha} \approx p^2 \frac{T_1}{\omega_{1s} - \omega - i/T_2} \approx p^2 T_1 T_2 \tag{125}$$

and assuming size-independent relaxation times, this ratio becomes almost size-independent (averaging over the size distribution slightly complicates the result). There have been experimental studies that roughly confirm this behavior [80, 81] (see also Fig. 12a,b).

The case of the Coulomb-mediated nonlinearity is more complex and can be treated analytically only under certain simplifications concerning the Coulomb interaction between electron-hole pairs. Banyai *et al.* [77], extending Takagahara's [75] approach, derived an expression for $\chi^{(3)}(\omega, -\omega, \omega)$ for

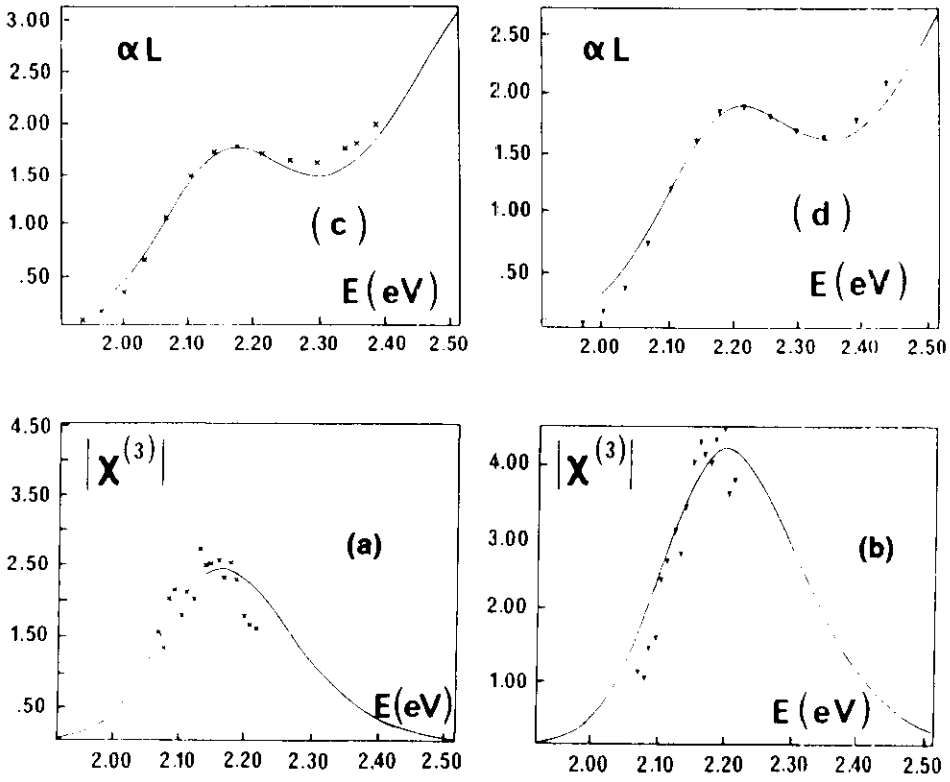

Fig. 12. Semilog plot of the imaginary part of $\chi^{(3)}$ and the absorption for two different semiconductor doped glass samples with crystallites of two different average sizes (from Refs. 90 and 91).

ω close to ω_{1s}, which we reproduce here:

$$\chi^{(3)} = \frac{1}{4V}\left\{\frac{4a^2\tau^2}{(\omega_{1s} - \omega) - i/\tau}\,\frac{1}{1 + (\omega_{1s} - \omega)\tau^2}\right.$$
$$-\beta^2\left\{\frac{2\tau^2}{(\omega_2 - \omega_{1s} - \omega) - i/\tau}\,\frac{1}{1 + (\omega_{1s} - \omega)^2\tau^2}\right.$$
$$+\frac{1}{(\omega_{1s} - \omega) - i/\tau}\,\frac{1}{(\omega_2 - 2\omega) - i/\tau}$$
$$\left.\left.\times\left[\frac{1}{(\omega_2 - \omega_{1s} - \omega) - i/\tau} - \frac{1}{(\omega_{1s} - \omega) - i/\tau}\right]\right\}\right\}, \tag{126}$$

while $\chi^{(1)}(\omega)$ is the same as in (124); ω_{1s} and ω_2 are the transition frequencies for one and two electron–hole pairs, respectively, A and B are the corresponding transition dipole moments,

$$A = |\langle 0|er|1s\rangle|^2, \tag{127}$$

$$B = |\langle 0|p|1s\rangle\langle 1s|p|2\rangle|, \tag{128}$$

and τ is a phenomenological relaxation time independent of the nature of the damping processes. The latter is a very drastic simplification that actually unduly exaggerates the impact of the Coulomb interaction, which, as can be inferred from (127), introduces an asymmetry above and below the resonance frequency ω_{1s} (see Fig. 13). The parameters B and ω_2 cannot be easily evaluated or extracted from experiment, and the size distribution in actual composities actually averages out most of the effects. For $B = 0$ and $\omega_2 = 2\omega$, (126) reduces to (122) after redefinition of certain parameters and setting $T_2 = T_1$.

As can be seen in (126), the main consequence of (the e h pair pair interaction) is that the optimally resonant susceptibility is not $\chi^{(3)}(\omega, \omega, \omega)$ with $\omega \approx \omega_{1s}$, but rather $\chi^{(3)}(\omega, -\omega, \omega')$, where $\omega' \approx \omega_2 - \omega_{1s}$ and $\omega_1 \approx \omega_{1s}$. As stated in the preceding, the impurity dominated nonlinearity also shows similar frequency behavior, and it is therefore difficult to distinguish the two merely by studying their frequency behavior. Rather, one must resort to time resolved studies to differentiate between the two.

The characteristic size dependence of $\chi^{(3)}$ for small semiconductor crystallites as derived in the preceding is due to the interband quantum confinement, and is valid for crystallite sizes smaller than the electron radius but larger than the unit cell. There has been a great deal of interest in the nonlinear optical properties of the crystallites when the crystallite radius is larger than the electron radius, as is the case in practice for CuCl crystallites, where the electron radius $a_e \approx 8$ Å. The initial treatment of the problem [76], introducing the coherent extension of the exciton wavefunctions and using the superradiant state approach, indicated that the nonlinear coefficient $\chi^{(3)}$ grows in proportion to the crystallite size. A careful analysis [82, 83], however

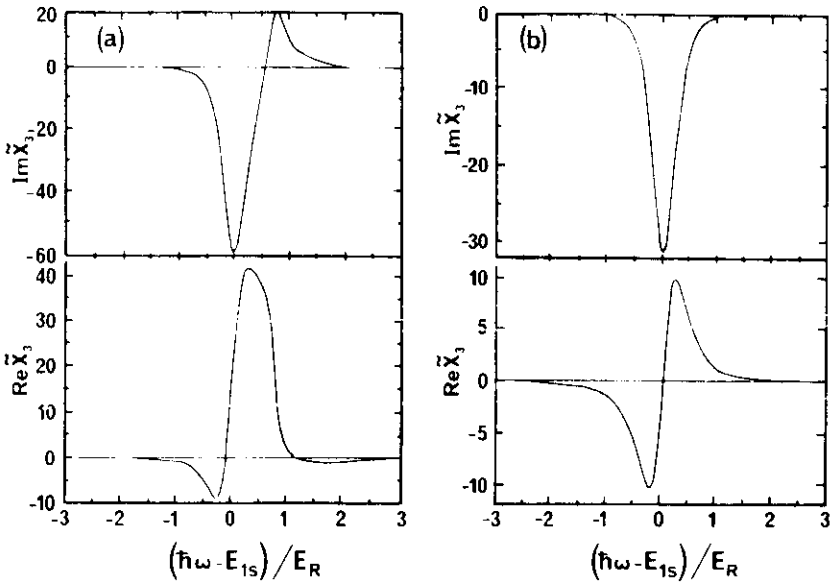

Fig. 13. Real and imaginary parts of $\chi^{(3)}$ in the strong confinement (b) and intermediate confinement (a) regimes showing the influence of Coulomb effects. E_R is the Rydberg energy of the exciton (from Ref. 77).

showed that this claim was incorrect and traced back to the unphysical way that the third order dipole moment induced at a given site inside the crystallite was related to the three electric fields acting on three different sites. The analysis of Refs. 82 and 83 clearly showed that all size-dependent contributions cancel out as the crystallite size grows.

5.2. Parametric Effects of Electroabsorption: The Quantum Confined Franz–Keldysh Effect

The previous discussion concerned changes in the absorption and index of refraction at frequency ω induced by a light field of intensity $I_{\omega'}$ at frequency ω', which in the most favorable case is either equal (degenerate) or close to ω (nearly degenerate). These changes are related to an effective light-intensity-dependent susceptibility $\chi(\omega; I_{\omega'})$, which also is defined by the relation

$$P_\omega = \chi(\omega; I_{\omega'})E_\omega \tag{129}$$

between the induced total polarization and the applied field, both at frequency ω (the roles of ω and ω' can be int changed), which for low intensities $I_{\omega'}$ reduces to the third-order polarization. Thus, $I_{\omega'}$, in a certain sense, plays the role of an external parameter that acts to modify the spectrum and dynamics

of the system (129), which can be viewed as a special case of a parametric process. There is a whole host of other external parameters that may change the spectral features, and by the same token the absorption and index of refraction. One such parametric process is of particular interest, namely changes in the absorption induced by the static electric field E_0, which can be formally considered as a special case of a field of frequency $\omega' = 0$ although its effect cannot be easily deduced by taking the limit $\omega' \to 0$ in the previous expressions. This is because in the previous discussion, by working close to resonances, we tacitly ignored certain contributions, and in particular we assumed that $\mu E < E_c$, where μ is the transition dipole moment and E_c measures the level spacing in the quantum confined structure as given by (15).

The effect of a static electric field E_0 in a bulk semiconductor gives rise to the Franz–Keldysh effect [84, 85], whose main characteristics are the appearance of an absorption tail [86] well inside the forbidden band gap and a modification of the ideally parabolic shape of the absorption onset in E_0, the critical region in the joint density of states of an ideal semiconductor. In the case of an atom, the same static electric field leads [87] to the static Stark effect, whose main characteristic is a shift of the atomic levels, which in the case of an ideal two-level atomic system leads to a repulsion of the two levels, and consequently to an increase of the apparent two-level separation. If we momentarily view an ideal two-band semiconductor as resulting from a periodic array of mutually interacting two-level atomic systems (see Fig. 7) whose closest neighbors' interaction strength also gives the band widths, we see that the applied static electric field leads to strikingly different effects in delocalized and localized electronic states: an attraction of interband levels close to the critical region, and a repulsion of the localized states, respectively. At a closer examination, it turns out that the underlying mechanism is one and the same as what was hinted in Section 3, namely replusion of states taken in pairs. In the case of delocalized band states, this has a different impact on the interband and intraband transitions. In the former, it leads to a global repulsion of the centers of gravity of the two bands, which can roughly be accounted for as a static Stark effect by using perturbation theory. The latter however, because of the close spacing (essentially vanishing) of the intraband levels, need a particular treatment and are the transitions that impose the conspicuous behavior close to the critical points, as observed in the Franz–Keldysh effect [86].

Since the quantum confinement precisely modifies the intraband spectrum, we expect that the Franz–Keldysh effect will be affected by the confinement, and in particular will evolve to a static Stark-like effect as the extension of the confinement is reduced. This is indeed corroborated both by the theoretical [88, 89] and experimental [90] studies.

The theoretical analysis [88] of electroabsorption in square quantum wells acted upon by a static electric field allowed the close relation between the

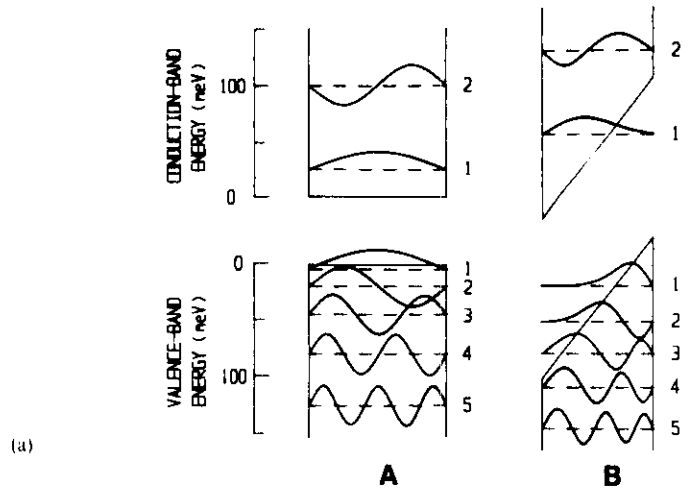

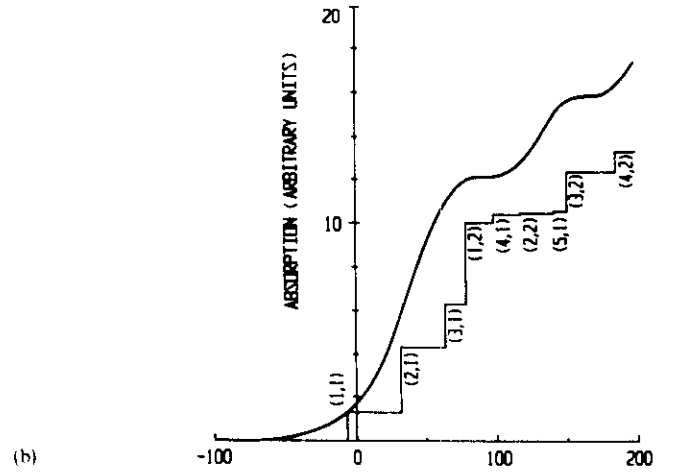

Fig. 14. (a) Valence and conduction energy levels and normalized wavefunctions for a square (A) and triangular quantum well (B). (b) Absorption of a finite (stepped line) and an infinitely thick (smooth curve) slab. The steps are labelled by their hole and electron quantum numbers. (c) Absorption of finite (long-dashed and short-dashed lines) and infinitely thick (full line) slabs for zero electric field. (d) Same as (c) for finite static electric field E_0 (from Ref. 88).

static Stark and Franz-Keldysh effects to be clearly shown. In the case of one-dimensional confinement using a square well potential (75), and introducing the effect of the static electric field in the Schrödinger equation as a term

$$H' = e(z_e - z_h)E_0. \tag{130}$$

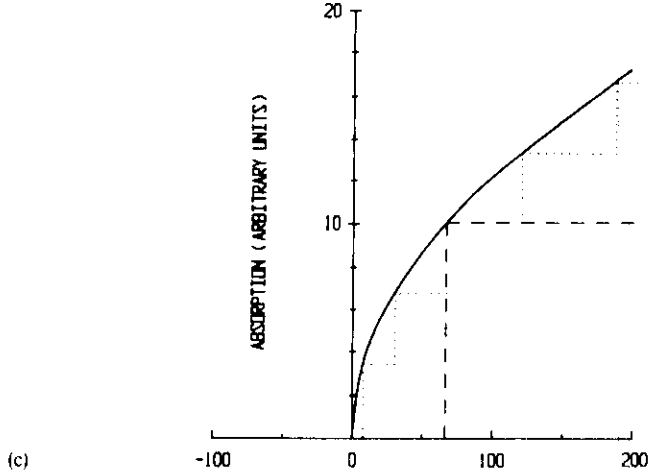

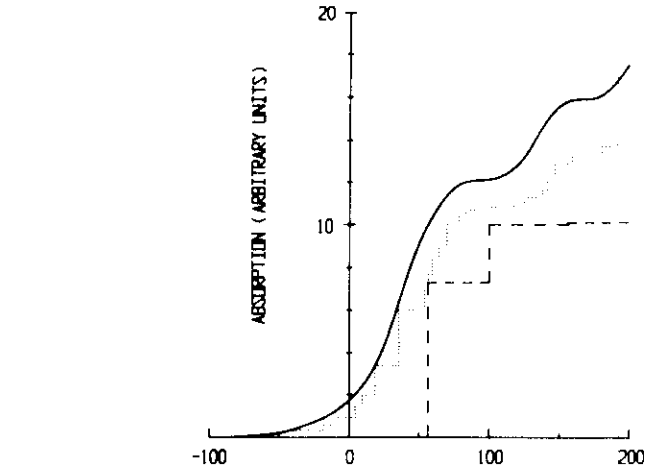

Fig. 14 (*continued*)

and neglecting the electron–hole interaction altogether, the analysis simply reduces [88] to the calculation of the absorption spectrum of a triangular potential well that is given by the solution of (78). The complete mathematical analysis can be found in Ref. 88, where numerical results are also presented. In Figs. 14a–d, we reproduce [88] such a calculation, which strikingly shows how the spectral modifications give rise to the bulk and quantum confined Franz-Keldysh effect, and how the latter evolves to the former as the confinement extension is increased.

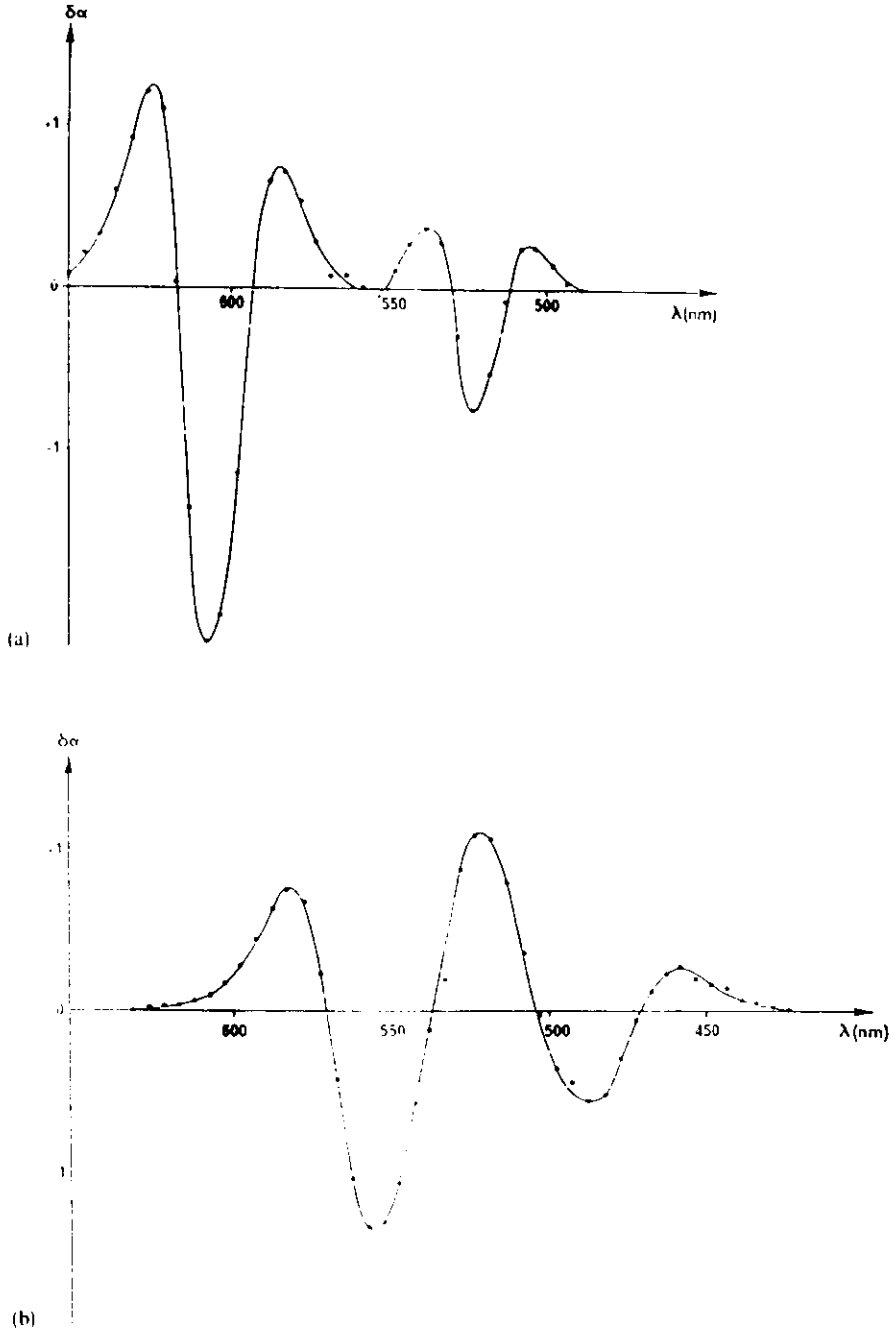

Fig. 15. Differential absorption spectra induced by a static field E_0 for particles of radii sizes of mean radius (a) 5 nm, (b) 3 nm, and (c) 1.5 nm (from Ref. 90).

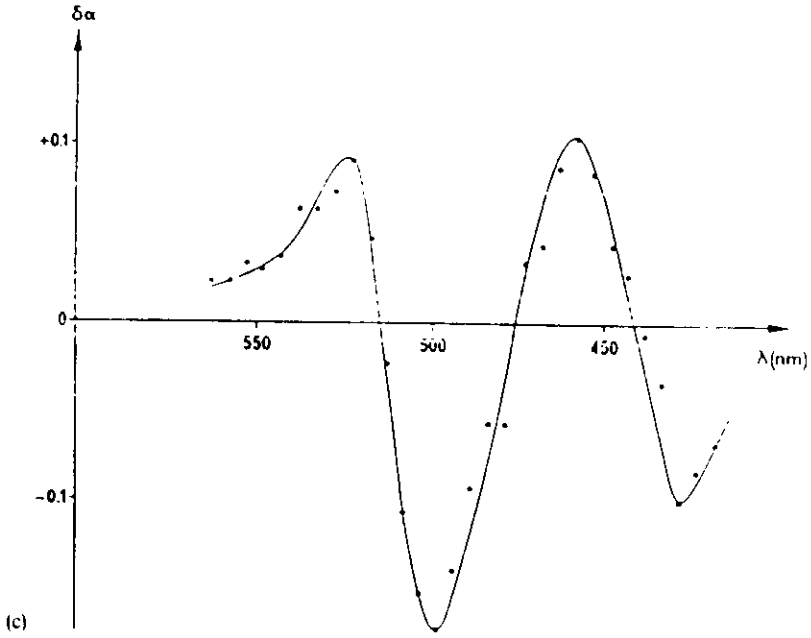

Fig. 15 (*continued*)

In the case of three-dimensional confinement, or quantum dot, the problem can be tackled [89, 90] along the same lines, and reduces to the solution of the Schrödinger equation of the envelope,

$$H = -\frac{\hbar^2}{2m_i^*}\nabla_i^2 + W(r_i) - e_i\mathbf{r}_i \cdot \mathbf{E}_0, \tag{131}$$

with i = e,h, which for $eLE_0/2 \ll E_c$ can be treated by Rayleigh–Schrödinger perturbation approach (one usually neglects the electron–hole interaction in calculating the effect of the static field E_0). The main features are that any nl state is now mixed with all $n'(l \pm 1)$ ones, and its energy is shifted by an amount proportional to E_0^2. In particular, its $2l + 1$ degeneracy is partially broken and gives rise to $l + 1$ distinct levels, each with double degeneracy. As a consequence, new transitions now appear with oscillator strengths borrowed from the initially allowed transitions in the absence of the static electric field. The oscillator strength of the latter is reduced in the presence of E_0 because of the incomplete overlap of the electron and hole envelopes. The compound effect of this rearrangement is the appearance of oscillations in the differential absorption coefficient $\delta\alpha = \alpha(\omega; E_0) - \alpha(\omega; 0)$, whose period should reflect the

confined level spacing. All of these features are the same as the those expected in the static Stark effect in atoms or molecules. One can also write

$$\delta\alpha = 12\pi\omega \operatorname{Im} \chi^{(3)}(0,0,\omega) E_0^2/nc \tag{132}$$

and get the value of the static Kerr effect susceptibility $\chi^{(3)}(0,0,\omega)$.

As the crystallite size increases, the condition $\mu E_0 < E_c$ will eventually cease to be valid and one must resort [89] to a nonperturbative solution of the problem along the lines of the treatment used for the one-dimensional square well potential [88] and for the bulk semiconductor [85].

Before discussing the experimental observations, we wish to complete the preceding discussion with the following remarks. The restriction to the two-band model can actually be relaxed by also introducing the spin-orbit split-off valence band. Besides the two-band contributions as before, one may also have three-band contributions and in addition the electron-hole interaction, which substantially complicate the treatment.

The experimental studies [90,91] of the electroabsorption in small quantum confined semiconductor crystallites strikingly corroborated the previous trends, and in particular the two main features. First, the displacement of the energy levels induces a shift of the elementary absorption peaks, which is also accompanied by a decrease of the oscillator strength as the overlap between hole and electron wave functions is decreased. Second, due to the breakdown of inversion symmetry and mixing of states, new transitions appear. As a consequence, the absorption change $\delta\alpha = \alpha(E_0) - \alpha(0)$ shows oscillations with spacing that depend on the crystallite size. Furthermore, this modification varies as E_0^2. In Fig. 15, we show the representative electroabsorption measurement series for three different sizes, which corroborate these predictions. As expected from quantum confinement, the whole structure broadens and blue shifts as the radius is decreased. All these observations clearly indicate that one has a static Stark effect. For the large crystallites, one sees [90] a replica of the oscillations due to the spin-orbit split-off valence band. This is also visible for the intermediate size crystallites but disappears in the smallest size particles because of the increased broadening or the valence band mixing.

The experimental behavior can also be quantitatively produced [90], as shown in Fig. 16. There, the results of the calculation of the absorption change $\delta\alpha$ and the absorption coefficient α for a small crystallite are shown. In the calculation, both level broadening and size dispersion were taken into account.

The preceding results confirm the interpretation of the electroabsorption as a static Stark effect for quantum confined crystallites. As the crystallite size increases and one recovers the band states, one expects that the electroabsorption will start revealing its Franz-Keldysh effect signature. This was experimentally confirmed [91]. These observations also confirm that the

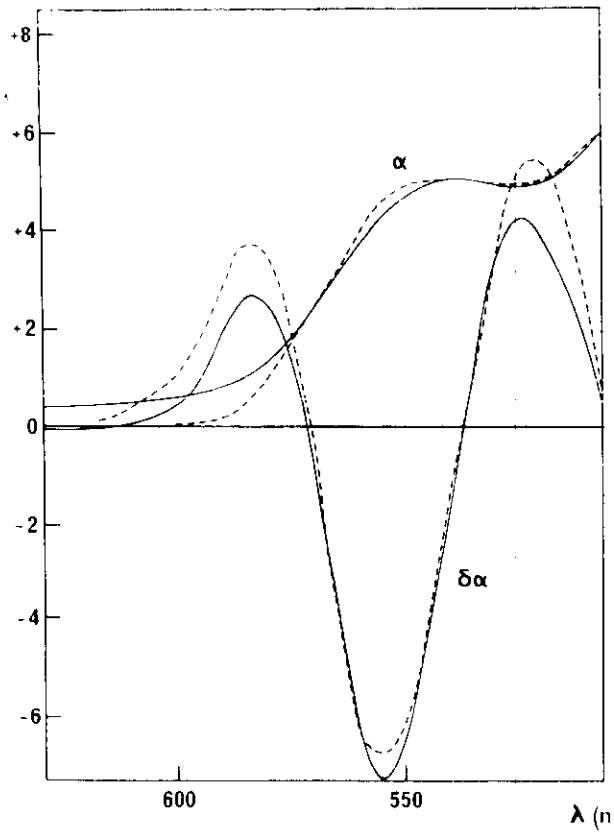

Fig. 16. Comparison between measurements (dashed lines) and perturbation theory calculation (solid lines) for a sample corresponding to (b) in Fig. 15 (from Ref. 90).

same microscopic mechanisms underlie the two effects as pointed out in the preceding.

Clearly, there are numerous other nonlinear and parametric processes that can be affected by the quantum confinement, and discussed along similar lines. Of particular interest and closely related with the previous processes are the two-photon absorption [92], the optical Stark effect [93], and Raman scattering [94], but also magnetooptical, piezooptic, and thermooptic effects can be of particular interest and will certainly be properly addressed in the near future. We shall conclude with a few remarks on second-order optical processes, which can only occur if the system macroscopically does not possess the inversion symmetry.

5.3. Second-Order Nonlinearities

In the previous discussion, we tacitly ignored that quantum confined structures may lack inversion symmetry and this for two reasons: (i) The semiconductor material by its intrinsic chemical and crystalline structure may lack inversion symmetry, and this is the case in all III-V, II-VI, and I-VII compounds. (ii) The confining potential well may be asymmetric, the simplest cases being the triangular potential well and the asymmetric double square well potential. In the first case, the asymmetry is related to the intracell charge asymmetry, and is not affected by the confinement since the latter extends over several unit cells. In the second case, on the other hand, the asymmetry can be affected and clearly depends on the details of the asymmetry of the potential, which substantially complicates its quantitative treatment. We shall restrict ourselves to some general remarks. It is important to point out that for a second-order optical process to take place, such as second harmonic generation, optical rectification, or linear Pockels effect, a macroscopic array of such asymmetric quantum confined structures must also lack inversion symmetry. If these structures form a periodic array and in addition are coupled, the situation gets complicated because "bands" may be formed out of the quantum confined states. If they are uncoupled, one may assume additivity for β, and concentrate on its magnitude for a single quantum well. This case can be analytically treated to a large extent, as the asymmetric potential has simple forms: triangular, asymmetric double well, or a well with a step.

The relevant quantity is the second-order polarizability $\beta(\omega_1, \omega_2)$, whose magnitude clearly depends on the potential asymmetry and on whether ω_1 and ω_2 are close to any of the quantum confined resonances. In the latter case, only the resonant term in (38) needs to be considered, and the behavior can be extracted by computing the relevant transition dipole elements [94, 95]; there are experimental investigations and estimations for the resonant rectification effect [96]. When ω_1 and ω_2 are well below any resonances expression, (42b) must be computed, which *a priori* implies the knowledge of all level spacings and dipole transition elements, which are both intra- and interband, (60) and (72), respectively. Actually, powerful perturbation techniques similar to the ones applied to calculate molecular second-order polarizabilities [7] can be extended and used here too to calculate $\beta(0, 0)$. An order of magnitude can be obtained by applying [97] the Unsöld approximation, which amounts to approximating all energy spacings by an average one, which can be calculated by making the same approximation in the sum rule for oscillator strengths,

$$\frac{2m}{\hbar^2} \sum_i |\mu_{ij}|^2 = 1. \tag{134}$$

A complication arises here because of interband and intraband transitions,

and the rise of the effective mass, and care must be paid to properly take into account the corresponding contributions. We shall not pursue this discussion any further except to point out that for a family of potential wells of the same shape but different effective asymmetry strength η, which can be defined by

$$\eta L = \int \mathbf{r}\rho(\mathbf{r})\, dV, \tag{135}$$

where $\rho(\mathbf{r})$ is the charge density distribution in the quantum confined structure and can vary from 0 to 1, there is an optimal second-order nonlinearity [98] for an intermediate value of η; this can be estimated to be $\eta \approx 1/\sqrt{7}$ since for the extreme cases of $\eta = 0$ and $\eta = 1$ one has symmetric quantum wells and $\beta = 0$. Such an optimal second-order susceptibility was initially point out in Ref. 98 for an isoelectronic semiconductor family. We wish to point out that in contrast to the second-order polarizability β, which shows such an optimal behavior and therefore is bound, for the third-order polarizability one cannot use similar or other considerations for its optimization.

6. GENERAL REMARKS AND CONCLUSIONS

In the previous treatment, we have purposely concentrated our discussion on the most elementary aspects of the quantum confinement, as these pertain in the strong confinement limit where the electron and hole motions are totally uncoupled, and we have shown that one has two types of quantum confinement, the intraband and interband, with quite distinct impacts on the optical nonlinearities. Only the former leads to size-dependent effects, while the latter does not, and this can be simply taken into account by using the expressions of the polarizabilities as in the case of atoms or molecules in the one-electron picture.

Beyond this regime, namely when electron–hole interaction is relevant, one must resort to Hartee or Hartree–Fock perturbation techniques, which greatly complicate the quantitative treatment. There have been some calculations along these lines, but the interpretation of experimental observations cannot be considered altogether satisfactory.

Along with these fundamental aspects of the nonlinear optical properties of quantum confined structures, the impact of the quantum confinement on the efficiency of several optical processes of potential use in devices still is a point of debate. It is quite evident that the figure of merit is not substantially improved by the quantum confinement since the ratio is quite insensitive to the number of electrons involved in an energy range, and this is precisely the only feature that changes in the interband confinement, the oscillator strength being unaffected. The situation *a priori* is different when intraband confinement is involved. However, in the case of semiconductors this quite often

implies the use of resonances between excited states, with all complications related to lifetimes, and in the case of metals this contribution is dominated by others insensitive to quantum confinement. Clearly, much work is still needed to understand the dynamics of the quantum confined states, and work in the future will concentrate on these aspects.

References

1. See, for instance, C. Flytzanis and J. L. Oudar, eds., "Nonlinear Optics: Materials and Devices," Springer-Verlag, 1986.
2. G. I. Stegeman and R. H. Stolen, "Waveguides and Fibers for Nonlinear Optics," preprint; see also D. Marcuse, "Theory of Dielectic Optical Waveguides," Academic Press, New York, 1974, or T. Tamir, ed., "Integrated Optics," Springer-Verlag, Berlin, 1975.
3. See, for instance, M. A. Reed and W. P. Pick, eds., "Nanostructure Physics and Fabrication," Academic Press, 1989.
4. See, for instance, C. Weisbuch and B. Vinter, "Quantum Semiconductor Structures: Fundamentals and Applications," Academic Press, 1991; see also J. C. Kelly and C. Weisbuch, eds., "Physics and Fabrication of Microstructures and Microdevices," Springer-Verlag, 1986.
5. See, for instance, G. Allan *et al.*, eds., "Heterojunctions and Semiconductor Superlattices," Springer-Verlag, 1986.
6. See, for instance, Y. R. Shen, "Principles of Nonlinear Optics," John Wiley, 1984.
7. See, for instance, C. Flytzanis, in "Quantum Electronics: A Treatise," Vol. 1a (H. Rabin and C. L. Tang, eds.), Academic Press, New York, 1975.
8. See, for instance, H. Heinrich, G. Bauer, and F. Kuchar, eds. "Physics and Technology of Submicron Structures," Springer-Verlag, 1988.
9. See, for instance, K. Kash, *J. Luminesc.* **46,** 69 (1990).
10. E. Kapon, M. C. Tamargo, and D. M. Huang, *Appl. Phys. Lett.* **50,** 347 (1987); W. T. Tsang and A. Y. Cho, *J. Appl. Phys.* **30,** 293 (1977).
11. P. M. Petroff, A. C. Gossard, and W. Wiegmann, *Appl. Phys. Lett.* **45,** 620 (1984).
12. H. M. Cox, P. S. Lin, A. Yi-Yan, K. Kash, M. Seto, and P. Bastos, *Appl. Phys. Lett.* **55,** 472 (1989); E. Colas, E. Kapon, S. Sumhony, H. M. Cox, R. Bhat, K. Kash, and P. S. Lin, *Appl. Phys. Lett.* **55,** 867 (1989).
13. For an extensive survey, see C. Flytzanis, F. Hache, M. C. Klein, D. Ricard, and Ph. Roussignol, "Nonlinear Optics in Composite Materials I, Semiconductor and Metal Crystallites in Dielectrics," Progress in Optics, Vol. (Wolf, ed.). Elsevier, 1991.
14. K. F. Renitz, N. Neuroth, and B. Speit, "Fabrication and Optical Specifications of Semiconductor Doped Glasses," Schott Glasswerke Research Report, Mainz, Germany, 1989.
15. See, for instance, C. R. Bumford," Colour Generation and Control in Glass," Elsevier, Amsterdam, 1977.
16. A. I. Ekimov, A. A. Onushchenko, and V. A. Tsekhomskii, *Fiz. Khim. Stekla* **6,** 511 (1980).
17. T. Itoh and T. Kurhavar, *J. Lum.* **31,** 120 (1984).
18. Y. Wang and N. Herron, *J. Phys. Chem.* **91,** 257 (1987); *ibid.* **91,** 5005 (1987); J. B. Parise, J. McDougall, N. Herron, R. Farlee, A. W. Sleight, Y. Wang, T. Bein, K. Meller, and L. M. Moroney, *Inorg. Chem.* **27,** 221 (1988); Y. Wang, A. Suna, W. Mahler, and R. Kasowskii, *J. Chem. Phys.* **87,** 7315 (1987).
19. M. Lucas, *Bull. Soc. Chim. Fr. (France)* **15,** 40 (1986); T. Ewan, *J. Soc. Chem. Ind. (London)* **10,** 10 (1909); C. B. Berry, *Phys. Rev.* **161,** 848 (1967).

20. A. Henglein, Ber. Buxsenges, *Phys. Chem.* **86,** 241 (1982).
21. R. Rossetti, S. Nakahara, and L. E. Brus, *J. Chem. Phys.* **79,** 186 (1983).
22. A. J. Nozik, F. Williams, M. T. Neviadovic, T. Rajh, and O. Micic, *J. Phys. Chem.* **89,** 397 (1985).
23. For a detailed and up to date discussion of metal particles in noncrystalline media, see J. A. A. J. Perenboom, J. Wyder, and F. Meier, *Phys. Reports* **78,** 173–292 (1981); and in crystalline solids, see A. E. Hughes and S. C. Jain, *Adv. Phys.* **28,** 717 (1979); see also W. P. Halperin, *Rev. Mod. Phys.* **58,** 533 (1986).
24. R. Kubo, *J. Phys. Soc. Japan* **17,** 975 (1962).
25. L. P. Gorkov and G. M. Eliashberg, *Zh. Eksp, Teor. Fiz.* **48,** 1407 (1965).
26. See, for instance, W. Ashcroft and N. D. Mermin, "Solid State Physics," Holt-Sauders, Tokyo, 1981, or W. A. Harrison, "Electronic Structure and the Properties of Solids," W. H. Freeman, London, 1980; see also J. C. Phillips, "Bonds and Bands in Semiconductors," Academic Press, New York, 1973.
27. R. S. Knox, "Theory of Excitons," (Solid State Phys., Suppl. 5), Academic Press, New York, 1963.
28. See, for instance, H. Haug, ed., "Optical Nonlinearities and Instabilities in Semiconductors," Academic Press, New York, 1988.
29. S. Schmitt-Rink, D. S. Chemla, and D. A. B. Miller, Adv. Phys. **38,** 89 (1989).
30. G. Bastard, "Wave Mechanics applied to Semiconductor Heterostructures," Editions de Physique, Paris, 1988. For a very detailed account of the application of the envelope wavefunction approximation in confined structures, see M. Altarelli in Ref. 5.
31. See, for instance, P. E. Lippens and M. Lanoo, *Phys. Rev. B* **39,** 10935 (1989).
32. See, for instance, C. J. Böttcher, "Theory of Electric Polarization," Elsevier, Amsterdam, 1973, or J. D. Jackson, "Classical Electrodynamics," John Wiley, New York, 1980.
33. K. C. Rustagi and C. Flytzanis, *Opt. Lett.* **9,** 344 (1984).
34. J. C. Maxwell-Garnett, *Philos. Trans. R. Soc. (London)* **203,** 385 (1904); *ibid* **205,** 237 (1906).
35. D. Ricard, Ph. Roussignol, and C. Flytzanis, *Opt. Lett.* **10,** 511 (1985).
36. G. S. Agarwal and S. Dutta Gupta, *Phys. Rev. A* **38,** 5678 (1988).
37. J. W. Haus, N. Kalyanivalla, R. Inguva, M. Bloemer, and C. M. Bowden, *J. Opt. Soc. Am. B* **6,** 797 (1989).
38. F. Hache, Thèse, Université de Paris, Orsay, 1988.
39. K. M. Leung, *Phys. Rev. A* **33,** 2461 (1986); D. S. Chemla and D. A. B. Miller, *Opt. Lett.* **11,** 522 (1986).
40. E. Blount, in Solid State Physics," Vol. 13 (F. Seitz and D. Turnbul, eds.), Academic Press, 1962.
41. P. N. Butcher and T. P. McLean, *Proc. Phys. Soc. (London)* **81,** 219 (1963).
42. D. E. Aspnes and J. E. Rowe, *Phys. Rev. B* **5,** 4022 (1972); D. E. Aspnes, *Phys. Rev. B* **6,** 4648 (1972).
43. V. N. Genkin and P. M. Mednis, *Sov. Phys. JETP* **27,** 609 (1968).
44. C. Cojan, G. P. Agrawal, and C. Flytzanis, *Phys. Rev. B* **15,** 909 (1977); G. P. Agrawal, C. Cojan, and C. Flytzanis, *Phys. Rev. B* **17,** 776 (1978).
45. C. Kittle, "Introduction to Solid State Physics," John Wiley, New York, 1988.
46. P. A. Wolf and S. A. Pearson, *Phys. Rev. Lett.* **17,** 1015 (1966); C. K. N. Patel, R. E. Slusher, and P. A. Fleury, *Phys. Rev. Lett.* **17,** 1011 (1966); A. A. Grinberg; *Sov. Phys. Solid State* **9,** 2004 (1988).
47. C. Flytzanis, in "Nonlinear Optical Properties of Organic Molecules and Crystals" (D. Chemla and J. Zyss, eds.), John Wiley, New York, 1987, and in "Nonlinear Optical Effects in Organic Polymers" (J. Messier, F. Kajzar, and P. Prasad, eds.), Kluwer, Amsterdam, 1989.

48. A. Kawabata and R. Kubo, *J. Phys. Soc. Japan* **21,** 1765 (1966); L. Genzel, T. P. Martin, and U. Kreibig, *Z. Phys. B* **21,** 339 (1975); R. Rupin and H. Yatom, *Phys. Stat. Sol. (b)* **74,** (1976); U. Kreibig and L. Genzel, *Surf. Sci.* **156,** 678 (1985).
49. E. J. Heilweil and R. M. Hochstrasser, *J. Chem. Phys.* **82,** 4762 (1985).
50. Al. L. Efros and A. L. Efros, *Sov. Phys. Semicond.* **16,** 772 (1982).
51. S. Schmitt-Rink, D. A. B. Miller, and D. S. Chemla, *Phys. Rev. B* **35,** 8113 (1987).
52. P. Roussignol, D. Ricard, C. Flytzanis, and N. Neuroth, *Phys. Rev. Lett.* **62,** 312 (1989); A. P. Alivisatos, T. D. Harris, P. J. Carroll, M. C. Steigerwald, and L. E. Brus, *J. Chem. Phys.* **90,** 3463 (1989).
53. M. Cardona, in "Spectroscopy of Semiconductor Microstructures" G. Fasol, A. Fasalino, and P. Lugli, eds.), Plenum Press, 1990.
54. P. Fauchet, in "Light Scattering in Semiconductor Structures and Superlattices" (D. J. Lockwood and J. F. Young, eds.), Plenum Press, 1990.
55. N. Mori and T. Ando, *Phys. Rev. B* **40,** 6175 (1989).
56. M. C. Klein, F. Hache, D. Ricard, and C. Flytzanis, *Phys. Rev.* **42,** 11123 (1990).
57. K. Huang and A. Rhys, *Proc. Roy. Soc. (London) A* **204,** 406 (1950); C. B. Duke and G. D. Mahan, *Phys. Rev.* **139,** 1965 (1965).
58. Y. Toyozawa, in "Polarons and Excitions" (G. Kuper and G. D. Whitfield, eds.), Oliver and Boyd, Edinburgh, 1963.
59. S. Lai and M. V. Klein, *Phys. Rev. Lett.* **44,** 1087 (1980); Z. Alferov, E. L. Portnoi, and A. A. Rogachev, *Sov. Phys. Semicond.* **2,** 1001 (1969); S. D. Baranowskii and A. L. Efros, *Sov. Phys. Semic.* **12,** 1328 (1978); C. Gourdon, Thèse d'Habilitation, Université de Paris, 1990.
60. See, for instance, D. Bohm, "Quantum Mechanics," Prentice-Hall, Englewood Cliffs, New Jersey, 1951, or E. Merzbacher, "Quantum Mechanics," John Wiley, New York, 1961.
61. J. Bardeen and W. Shockley, *Phys. Rev.* **80,** 72 (1950).
62. M. Cardona and F. H. Pollack, in "Optoelectronic Materials," (G. A. Albers, ed.), Plenum, New York, 1971.
63. G. P. Agrawal and C. Flytzanis, *Chem. Phys. Lett.* **44,** 366 (1976).
64. See, for instance, the books referred to in Ref. 47.
65. G. Wannier, *Rev. Mod. Phys.* **34,** 645 (1962).
66. H. Fukuyama, R. A. Bari, and B. Fogedby, *Phys. Rev. B* **8,** 5579 (1973).
67. K. Rustagi and J. Ducuing, *Opt. Comm.* **10,** 258 (1972); P. L. Davies, *Trans. Far. Soc.* **48,** 789 (1952).
68. H. Kuhn, *J. Chem. Phys.* **16,** 840 (1948).
69. J. N. Murrell, "The Theory of the Electronic Spectra of Organic Molecules," Methuen, London, 1963.
70. For a fairly clear summary concerning these points for the semiconductor crystallites, see M. Bawendi, M. L. Steigerwald, and L. E. Brus, *Ann. Rev. Phys. Chem.* **41,** 535 (1990).
71. J. Hutter and C. Flytzanis, in "Nonlinear Optical Properties of Organic Molecules and Polymers" (J. Kajar and J. Messier, eds.), Kluwer, Amsterdam, to appear.
72. I. M. Lifshitz and V. V. Slezov, *Sov. Phys. JETP* **8,** 331 (1959); see also I. M. Lifshitz and I. P. Pitaevskii, "Physical Kinetics," Pergamon Press, Oxford, 1987.
73. F. Hache, D. Ricard, and C. Flytzanis, *J. Opt. Soc. Am B* **3,** 1647 (1986).
74. F. Hache, D. Ricard, C. Flytzanis, and U. Kreibig, *Appl. Phys. A* **47,** 347 (1988).
75. T. Takagahara, *Phys. Rev. B* **36,** 9293 (1987).
76. E. Hanamura, *Phys. Rev. B* **37,** 1273 (1988); *Solid St. Comm.* **62,** 465 (1987).
77. L. Banyai, Y. Z. Hu, M. Lindberg, and S. W. Koch, *Phys. Rev. B* **38,** 8142 (1988); Y. Z. Hu, M. Lindberg, and S. W. Koch, *Phys. Rev. B* **42,** 1713 (1990).
78. N. Peyghambarian, B. Fluegel, D. Hulin, A. Migus, M. Joffre, A. Antonetti, S. W. Koch, and M. Lindberg, *IEEE J. Quant. Electron* **QE-25,** 2516 (1989).

79. M. G. Bawendi, W. L. Wilson, L. Rothberg, P. J. Carroll, T. M. Jedju, M. L. Steigerwald, and L. E. Brus, *Phys. Rev. Lett.* **65,** 1623 (1990).
80. Ph. Roussignol, Thèse (d'Etat), Université d'Orsay, 1989.
81. Ph. Roussignol, D. Ricard, and C. Flytzanis, *Appl. Phys. B* **51,** 437 (1990).
82. F. C. Spano and S. Mukamel, *Phys. Rev.* **40,** 5783 (1989).
83. H. Ishihara and K. Cho, *Phys. Rev. B* **42,** 1724 (1990).
84. W. Franz, *Z. Naturforschung A* **13,** 484 (1958).
85. L. V. Keldysh, *Sov. Phys. JETP* **7,** 788 (1958).
86. See, for instance, M. Cardona, "Modulation Spectroscopy," Academic Press, New York, 1969.
87. See, for instance, W. Demtröder, "Laser Spectroscopy," Springer-Verlag, Berlin, 1982.
88. D. A. B. Miller, D. S. Chemla, and S. Schmitt-Rink, *Phys. Rev.* **33,** 6979 (1986).
89. D. A. B. Miller, D. S. Chemla, and S. Schmitt-Rink, *Appl. Phys. Lett.* **52,** 2154 (1988).
90. F. Hache, D. Ricard, and C. Flytzanis, *Appl. Phys. Lett.* **55,** 1504 (1989).
91. D. Cotter and H. P. Girdlestone, Technical Digest IQEC, Anaheim, Paper QTu A 3, 1990.
92. R. Tommasi, M. Lepore, M. Ferrara, and I. M. Catalano (to be published).
93. S. Schmitt-Rink, D. S. Chemla, and H. Huang, *Phys. Rev. B* **37,** 941 (1988).
94. B. Tsang, D. Ahn, and S. L. Chuang, *Appl. Phys. Lett.* **52,** 697 (1988).
95. M. M. Fejer, S. J. B. Yao, R. L. Byer, A. Harwit, and J. S. Harris, Jr., *Phys. Lett.* **62,** 1041 (1989).
96. E. Rosencher, P. Bois, J. Nagle, E. Costard, and S. Delaitre, *Appl. Phys. Lett.* (to appear).
97. C. Flytzanis and J. Ducuing, *Phys. Rev.* **178,** 1218 (1969).
98. C. L. Tang and C. Flytzanis, *Phys. Rev. B* **4,** 2520 (1971).

THE ORIGIN OF THE OPTICAL NONLINEARITY OF Cd(S,Se)-DOPED GLASSES : ANOTHER APPROACH

M. Ghanassi, L. Piveteau, M.C. Schanne-Klein, D. Ricard

and C. Flytzanis

Laboratoire d'Optique Quantique du C.N.R.S.

Ecole Polytechnique, 91128 Palaiseau Cedex, France

Phone : +33 1 69 33 47 69

Fax : +33 1 69 33 30 17

Abstract : We show that by time resolving the nonlinear response of selenium-rich Cd(S,Se)-doped glasses with various degrees of photodarkening, we can clearly assess the origin of the resonant optical Kerr effect in these materials. Usually a combination of a fast free-carrier contribution and of a slow trapped-carrier one is observed. Their relative magnitude depends on the origin and on the past history of the sample.

The linear and nonlinear optical properties of semiconductor-doped glasses, mainly CdS, CdSe and CuCl corresponding to different confinement regimes, have been extensively studied in the last ten years [1,2]. Here we will concentrate on the strong confinement regime exemplified by CdSe or CdS_xSe_{1-x} alloys with a not too large value of x. In their case, the consequences of valence band degeneracy have been clearly established [3], the dynamics of free carrier recombination are well understood [4], the line broadening mechanisms have been studied [5-7] and estimations of the resonant Kerr susceptibility have been made assuming that a single mechanism is operative [1].

However, neither the range of applicability of the different mechanisms nor their relative contributions to the effective Kerr susceptibility have been clearly delineated. We know that carriers are created. We may then expect a nonlinear response due to the saturation of the ground state to one-pair excited state transition [8] and to induced absorption corresponding to interband transitions between the one-pair and a two-pair excited state or to intraband transitions. We will denote this mechanism the free carrier contribution. We also know that carriers may be trapped in long lived states and that these trapped carriers may also modify the optical properties of the semiconductor nanoparticles [9,10] either through the static electric field they create or through a phase space filling mechanism. This will be called the trapped carrier contribution.

Intensity-dependent measurements of the $\chi^{(3)}(\omega,-\omega,\omega)$ and of the $\chi^{(3)}(\omega,-\omega,\omega) / \alpha(\omega)$ spectra ($\chi^{(3)}(\omega,-\omega,\omega)$ is the degenerate Kerr susceptibility and $\alpha(\omega)$ is the absorption coefficient) carried out on $CdS_{0.4}Se_{0.6}$ doped samples using optical phase conjugation were interpreted as follows [11] : at low laser intensity, the dominant contribution is the trapped-carrier one whereas at higher laser intensity the free-carrier contribution becomes dominant. Here we address more quantitatively the relative contribution of these two mechanisms taking into account two aspects that have been overlooked in Ref.[11]. First, when the laser beam intensity is increased, the phase conjugate beam intensity saturates and is no longer proportional to the Kerr susceptibility squared. Secondly, frequency dependent measurements are not the clearest way of distinguishing the two contributions as we will see below.

In this letter, we will report on time-resolved measurements performed on samples having

experienced various degrees of photodarkening [12] which we feel more reliable. We will see that both mechanisms can contribute and that their relative magnitude depends on the sample and on its past history. The samples are either commercial Schott filters such as RG 630 or experimental samples having the same chemical composition as the RG 630 filters, x = 0.4. The technique is optical phase conjugation with copolarized forward pump and probe beams (the pulses being time coincident) which create a population grating which is probed by a cross-polarized backward pump beam. The diffracted (phase conjugate) pulse energy is measured. The laser intensity is always small enough in order to avoid saturation of phase conjugation. In time-resolved measurements, the backward pump pulse is delayed. We also performed frequency-dependent measurements by tuning the laser wavelength and working at "zero" delay i.e. when the conjugate pulse energy is maximum. The laser we used is a distributed feedback dye laser (DFDL) tunable between 560 and 610 nm and delivering a 25 psec pulse from which the three incident pulses are derived. It is pumped by the second harmonic (λ = 532 nm) of a Nd:YAG picosecond pulse. Most of the measurements reported here have been performed at room temperature.

The consequences of photodarkening [12] are now well known. The slow component of luminescence due to trapped carrier recombination is drastically reduced as if trapping centers were no longer existent or efficient, the nonlinear response becomes faster, the nonradiative decay rate of free carriers increases [4] and the "zero" delay $\chi^{(3)}$ decreases. The absorption spectrum is not significantly altered however. We took fresh samples and deliberately darkened them by exposing them to a laser beam at λ = 532 nm for 1-2 h. The darkening beam diameter was 2.5 mm with a gaussian profile, the pulse energy ≈ 0.6 mJ and the repetition rate 1 pulse per second. The laser beam diameter in the phase conjugation set-up was smaller (≈ 0.7 mm) so that we could probe spots on the sample having received various doses. Measuring $\chi^{(3)}$ at "zero" delay, as a function of position, we got results such as the one shown in Fig.1.

Fig.1 clearly shows how photodarkening reduces the magnitude of the measured susceptibility $\chi^{(3)}$. The ratio between $\chi^{(3)}$ for a nondarkened area and $\chi^{(3)}$ for the most darkened one is larger for a commercial glass than for an experimental one. We recall that for these samples, commercial ones have more trapping centers than experimental ones [13]. We

also observe that the decrease of $\chi^{(3)}$ can be fitted by a gaussian profile reproducing the 532 nm laser profile. The minimum value of $\chi^{(3)}$ does not decrease to zero. When the darkening dose is increased, we observe a saturation of darkening, the bottom of the $\chi^{(3)}$ profile becoming flat.

We then choose a given position of the sample and time-resolve the nonlinear response by delaying the backward pump pulse. Two typical results are shown in Fig.2, Fig.2a corresponding to a less darkened area and Fig.2b to a more darkened one. We clearly see that the nonlinear response is made of two components, a fast component decaying exponentially with a time constant varying between ~ 30 psec and ~ 1 nsec and a slow component whose decay constant is at least tens of nanoseconds. This is in agreement with previous observations (see Fig.1a of Ref.[14]). We notice that our set-up is not well suited to measure long decay times since the DFDL beam is not perfectly collimated. It is however quite reliable when the decay time is smaller than 1 nsec.

We now argue that the slow component corresponds to the trapped-carrier contribution whereas the fast component corresponds to the free-carrier one. The larger the darkening dose is, the smaller the time constant of the fast component and the smaller the relative magnitude C_s/C_f of the slow and fast components. One can get to the point where there is only a fast component : assuming C_s to be proportional to the number of active trapping centers, this would then mean that the trapping centers have been completely deactivated. On the contrary, when working with a fresh commercial sample in the exponential tail of the absorption spectrum such as OG 530 at λ = 532 nm, there is usually only a slow component. Near the $1s_h$-$1s_e$ transition (the substructure due to the $1S_{3/2}$ and $2S_{3/2}$ hole levels [3] is not visible for these samples) however, even for fresh samples, the nonlinear response is the sum of a fast and a slow component. The results shown in Fig.2 and those discussed above correspond to such a resonant regime.

If the fast component corresponds to free carriers and neglecting intraband transitions which are presumably weak, it is due to saturation of the $1s_h$-$1s_e$ transition and to induced absorption between this one-pair excited state and a two-pair excited state. The expression for such a $\chi_f^{(3)}$ is well known [15]. Keeping only the resonant two-pair state, the hyperpolarizability γ_f reads :

$$\gamma_f = -\frac{1}{4}\frac{4\,\mu_{10}^4 - 2\,\mu_{21}^2\,\mu_{10}^2}{\hbar^3\,(\delta^2+1)\,(\delta - i)}\,T_2^2\,T_1 \qquad (1)$$

where μ_{10} is the transition matrix element of the dipole moment between ground state $|0\rangle$ and one-pair state $|1\rangle$, μ_{21} is the transition matrix element between state $|1\rangle$ and the two-pair state $|2\rangle$, T_2 is the dephasing time assumed to be the same for the two transitions, $\delta = (\omega_{10} - \omega)T_2 = (\omega_{21} - \omega)T_2$ is the normalized detuning and T_1 is the lifetime of level $|1\rangle$. T_1 is the time constant of the fast component.

Using laser pulses of duration t_p (25 psec) smaller than the response times, we are in the transient regime and we measure an effective susceptibility. Its fast component C_f at "zero" delay and for rectangular pulses is related to the true $\chi_f^{(3)}$ by :

$$C_f = \chi_f^{(3)}\left[\frac{T_1}{t_p}\left[-\ln\left(1-(1-y)^2\right) - \frac{(1-y)^2}{2-y}\right]\right]^{1/2} \qquad (2)$$

where $y = \exp(-t_p/T_1)$. More detailed calculations will be given in a forthcoming publication. From the measured value of T_1 and of C_f, we can then get the value of $\chi_f^{(3)}$. Since photodarkening does not change the absorption spectrum, μ_{10}, δ, T_2 and presumably μ_{21} are not modified by photodarkening. Equation (1) then tells us that the ratio $\chi_f^{(3)}/T_1$ should be constant. Table I shows the values of T_1 and of the ratio $\chi_f^{(3)}/T_1$ for various degrees of darkening and we see that, within the experimental uncertainty, the ratio $\chi_f^{(3)}/T_1$ is indeed constant. (?)

For the range of values we measure for T_1, the fast component of the effective susceptibility C_f is roughly constant as can be seen in Table 1. If we assume that the slow component C_s is proportional to the number of still active trapping centers, then we understand why the $\chi^{(3)}$ (or C_s+C_f) profile in Fig.1 follows the intensity profile of the darkening laser beam : the number of deactivated centers is simply proportional to the radiation dose. We also notice that the measured $\chi_f^{(3)}$ is about 100 times weaker than the value one would get by neglecting the second term in eqn (1), i.e. by neglecting induced absorption between the one-pair state and two-pair states. Induced absorption has been observed in the nondegenerate case

[6] and our results indicate that, in the degenerate case, it leads to an important cancellation effect.

Working at "zero" delay, we also measured the $\chi^{(3)}/\alpha$ spectrum. A typical result is shown in Fig.3. In the exponential tail of the absorption spectrum, the ratio $\chi^{(3)}/\alpha$ is observed to be frequency independent but the reason for this is still unclear. We also observe a resonance in the vicinity of the $1s_h$-$1s_e$ transition. This is in agreement with previous observations [16] : notice that, in Fig.2 of Ref.[16], the logarithm of $\chi^{(3)}$ is plotted whereas in Fig.3 a linear plot is shown. We observe that this resonance is more apparent for experimental samples for which the transition is narrower. It is also sharper at liquid nitrogen temperature than at room temperature. We recall that, at room temperature, the broadening is mainly homogeneous or intrinsic and that the width of the $1s_h$-$1s_e$ feature in the absorption spectrum decreases when the temperature is reduced [7].

In the vicinity of the resonance, the $\chi^{(3)}/\alpha$ spectrum is however about the same for a fresh and for a darkened sample when the nonlinear mechanism has changed as discussed above. A study of this $\chi^{(3)}/\alpha$ spectrum is not the best way of assessing the origin of the nonlinearity. In fact, as shown in eqn (1), $\chi^{(3)}/\alpha$ should exhibit a resonance in the vicinity of the $1s_h$-$1s_e$ transition for the free carrier contribution, at least when homogeneous broadening dominates. But, in the case of the trapped carrier contribution , although $\chi_s^{(3)}$ is proportional to the number of trapped carriers, assuming for example the nonlinearity to be due to the static electric field, $\chi_s^{(3)}$ is also proportional to the static $\chi^{(3)}(0,0,\omega)$ and the ratio $\chi^{(3)}/\alpha$ is also expected to show a resonance in the vicinity of the same transition [17].

In conclusion, we have shown that, by time resolving the nonlinear response of semiconductor-doped glasses having experienced various degrees of photodarkening, we are able to more clearly assess the origin of the resonant optical Kerr effect in these materials. In limiting cases, this nonlinearity is mainly due to only one contribution, trapped carriers or free carriers. More generally, it is the sum of these two contributions. The relative magnitude of the two contributions is difficult to assess a priori. The best way of determining it is to time resolve the nonlinear response at low enough intensity.

REFERENCES

1 - R.K. Jain and R.C. Lind

J. Opt. Soc. Am. 73, 647 (1983)

2 - C. Flytzanis, F. Hache, M.C. Klein, D. Ricard and P. Roussignol

in Progress in Optics, vol 29, E. Wolf ed. (North Holland, Amsterdam, 1991)

3 - A.I. Ekimov, F. Hache, M.C. Schanne-Klein, D. Ricard, C. Flytzanis, I.A. Kudryavtsev, T.V. Yazeva, A.V. Rodina and Al.L. Efros

J. Opt. Soc. Am. B 10, 100 (1993)

4 - M. Ghanassi, M.C. Schanne-Klein, F. Hache, A.I. Ekimov, D. Ricard and C. Flytzanis

Appl. Phys. Letters 62, 78 (1993)

5 - M.G. Bawendi, W.L. Wilson, L. Rothberg, P.J. Carroll, T.M. Jedju, M.L. Steigerwald and L.E. Brus

Phys. Rev. Letters 65, 1623 (1990)

6 - N. Peyghambarian, B. Fluegel, D. Hulin, A. Migus, M. Joffre, A. Antonetti, S.W. Koch and M. Lindberg

I.E.E.E. J. Quant. Electron. 25, 2516 (1989)

7 - P. Roussignol, D. Ricard, C. Flytzanis and N. Neuroth

Phys. Rev. Letters 62, 312 (1989)

8 - S. Schmitt-Rink, D.A.B. Miller and D.S. Chemla

Phys. Rev. B 35, 8113 (1987)

9 - P. Roussignol, D. Ricard, K.C. Rustagi and C. Flytzanis

Optics Commun. 55, 143 (1985)

10 - E.F. Hilinski, P.A. Lucas and Y. Wang

J. Chem. Phys. 89, 3435 (1988)

11 - M.C. Schanne-Klein, F. Hache, D. Ricard and C. Flytzanis

J. Opt. Soc. Am. B 9, 2234 (1992)

12 - P. Roussignol, D. Ricard, J. Lukasik and C. Flytzanis

J. Opt. Soc. Am. B 4, 5 (1987)

13 - F. Hache, M.C. Klein, D. Ricard and C. Flytzanis

J. Opt. Soc. Am. B 8, 1802 (1991)

14 - P. Roussignol, M. Kull, D. Ricard, F. de Rougemont, R. Frey and C. Flytzanis

Appl. Phys. Letters, 51, 1882 (1987) and erratum 54, 1705 (1989)

15 - L. Banyai, Y.Z. Hu, M. Lindberg and S.W. Koch

Phys. Rev. B 38, 8142 (1988)

16 - P. Roussignol, D. Ricard and C. Flytzanis

Appl. Phys. A 44, 285 (1987)

17 - F. Hache, D. Ricard and C. Flytzanis

Appl. Phys. Letters 55, 1504 (1989)

FIGURE CAPTIONS

Fig. 1 : The "zero" delay effective Kerr susceptibility plotted as a function of position for a sample which has been photodarkened with a laser beam having a gaussian profile and a diameter of 2.5 mm. The dots correspond to the experimental data and the solid line is a gaussian fit. One can notice a faint saturation of the darkening process.

Fig. 2 : The effective Kerr susceptibility, proportional to the square root of the conjugate pulse energy, plotted as a function of the backward pump pulse delay for (a) a less darkened area and (b) a more darkened one. The solid line is a fit with the sum of a fast exponential component and of a slow one.

Fig. 3 : Absorption $\alpha(\omega)$ spectrum and $\chi^{(3)} / \alpha$ spectrum for a fresh experimental sample with a mean particle radius of = 32 Å. $\chi^{(3)}$ is the "zero" delay effective susceptibility. From the second derivative of the $\alpha(\omega)$ spectrum, we know that the $1s_h$-$1s_e$ transition occurs around λ = 590 nm.

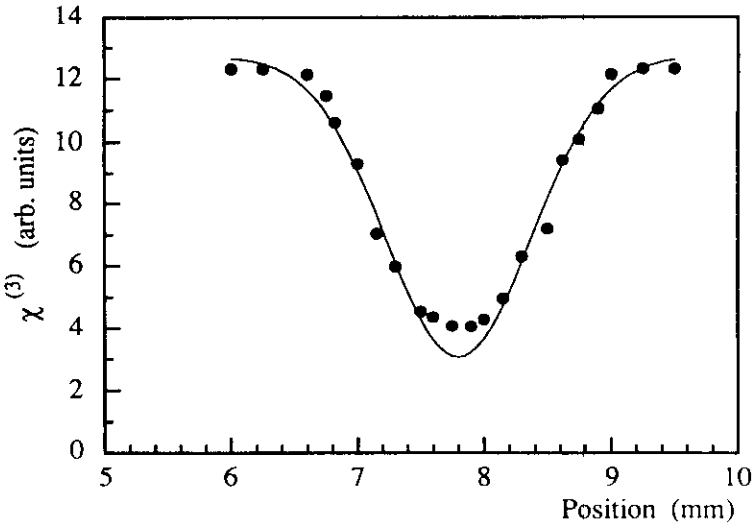

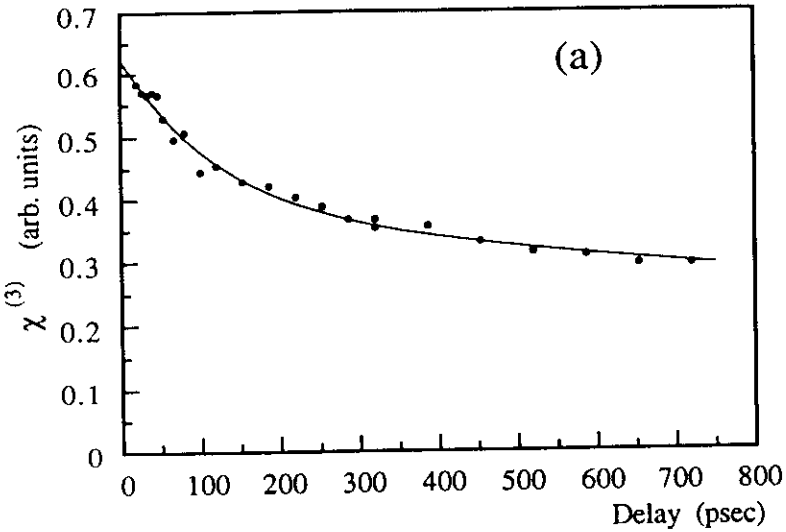
(a)
0.7
0.6
0.5
0.4
0.3
0.2
0.1
0
$\chi^{(3)}$ (arb. units)
0
100
200
300
400
500
600
700
800
Delay (psec)

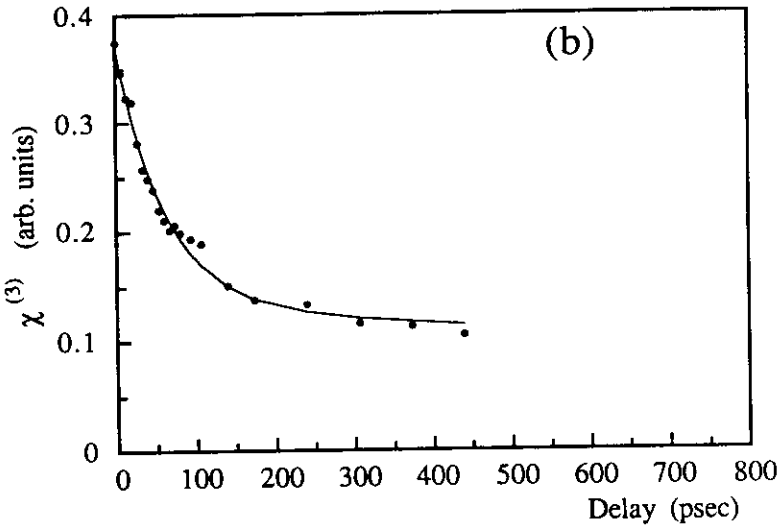
(b)
0.4
0.3
0.2
0.1
0
$\chi^{(3)}$ (arb. units)
0
100
200
300
400
500
600
700
800
Delay (psec)

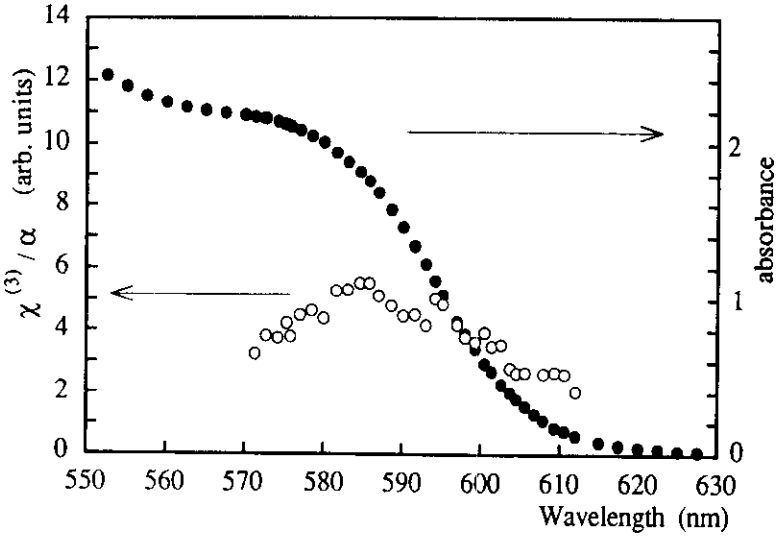
14
12
10
8
6
4
2
0
$\chi^{(3)}/\alpha$ (arb. units)
2
1
0
absorbance
550
560
570
580
590
600
610
620
630
Wavelength (nm)